AD-A090 629 NAVAL OCEAN RESEARCH AND DEVELOPMENT ACTIVITY NSTL S--ETC F/G 17/9
EASTERN ARCTIC SURSAT SAR ICE EXPERIMENT: RADAR SIGNATURES OF S--ETC(U)
AUG 80 R D KETCHUM, L D FARMER
UNCLASSIFIED NORDA-TN-68 NL

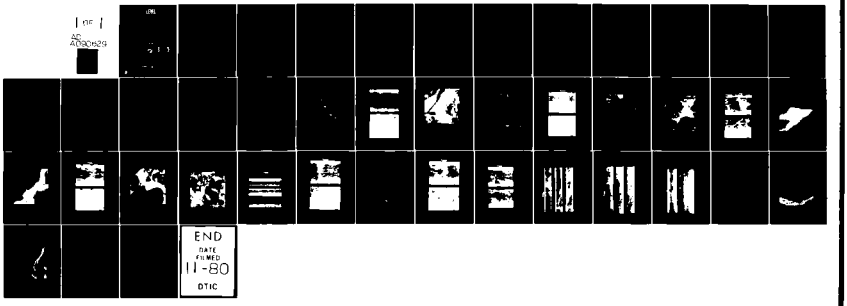

LEVEL II

NORDA-TN-

NORDA TECHNICAL NOTE 68

EASTERN ARCTIC SURSAT SAR ICE EXPERIMENT: RADAR SIGNATURES OF SEA ICE FEATURES

R.D. Ketchum, Jr. and L. Dennis Farmer

Oceanography Division

Ocean Science and Technology Laboratory

August 1980

NAVAL OCEAN RESEARCH AND DEVELOPMENT ACTIVITY

NSTL Station, Mississippi 39529

ABSTRACT

Evaluation of X- and L-band steep angle synthetic aperture radar (SAR) sea ice imagery taken in Baffin Bay and Davis Strait in April 1979 has shown that description and discrimination of first-season ice types can be difficult because of ambiguous radar returns. Ambiguous returns seen on X-band radar imagery are attributed to snow cover. The data have indicated that changes in snow properties due to melting and refreezing cause development of a highly reflective medium to the 3 cm X-band radar. The 25 cm L-band radar is not noticeably affected by the observed phenomena, thus correlation of coincident X- and L-band imagery often resolves interpretation ambiguities on the X-band imagery caused by the snow effects.

The data suggest that L-band radar energy often penetrates the ice and that subsurface returns are received. These returns also produce ambiguities in interpretation. Apparent smooth surfaces do not show this effect, but rough surfaces which have widely different roughness densities may produce apparently equal backscatter of L-band radar.

Ice ridge identification and discrimination was often poor due to the obscuring effects of background clutter associated with the above-suggested backscattering phenomena. Small ridge sizes versus system resolution and steep angles of incidence also reduce ridge identification capabilities.

Some icebergs produced time-delayed L-band signals, indicating internal reflections within the iceberg. Iceberg/water interface reflections rather than volume scattering are indicated. L-band radar cannot be depended upon for iceberg identification, since icebergs may be only partially imaged or not imaged at all by this frequency.

Table of Contents

INTRODUCTION

The Ice Experiment Plan of the Canadian Surveillance Satellite (SURSAT) Project was conducted during the winter and spring of 1979. This cooperative effort between Canada, the United States, and Denmark consisted of planned operational phases in four different geographic areas: the Gulf of St. Lawrence, the Beaufort Sea, the Eastern Arctic, and the Grand Banks. The Grand Banks phase was cancelled due to required aircraft and ship repairs.

The primary objective of the SURSAT Ice Experiment was to evaluate and to develop interpretation capabilities for dual-frequency, dual-polarized synthetic aperture radar (SAR) imagery of sea ice features and conditions. SURSAT and subsequent efforts will lead to an operational SAR that can be used to provide reports of ice conditions in real-time, to support ice forecasting, and also to serve as a system to support studies of sea ice dynamics.

This report discusses the collection and the analysis of data collected in April 1979 during the SURSAT Project Phase 3, which was conducted over ice-covered waters in the eastern Arctic. During this phase, the U.S. Navy's BIRDSEYE RP-3A aircraft, under the technical direction of the Naval Ocean Research and Development Activity (NORDA), flew jointly with the Canadian SAR-equipped aircraft to collect complementary data to aid in evaluation of the SAR data. The RP-3A aircraft was equipped with a Wild RC-8 cartographic camera, infrared line scanner, laser surface profiler, and PRT-5. The 9-inch (24 cm) photography obtained with the RC-8 camera provided the most useful data for cross-correlation and evaluation of the SAR imagery. The SAR system (INTERA Environmental Consultants, Ltd., 1978) was flown in a CONVAIR-580, owned by the Canada Centre for Remote Sensing. The Airborne SAR Project was managed by INTERA Environmental Consultants, Ltd., Ottawa, Canada.

Flight tracks were preselected by the SURSAT ice experiment team. Both aircraft were equipped with LTN-51 inertial navigation systems. The Navy RP-3A flight originally planned to fly 3.35 nautical miles to the starboard side of the Canadian CONVAIR-580 track in order to obtain the required coincident ice coverage. This procedure was not completely successful due to navigational errors. However, coincident coverage was obtained over areas having typically different ice conditions, thus providing adequate information for a useful evaluation of the four-channel SAR imagery.

Joint flights of the CONVAIR-580 and RP-3A aircraft were made during 8-13 April. The CONVAIR-580, with SAR system, flew at altitudes of 5200 and 5500 meters for optimum SAR coverage. The RP-3A flew at altitudes of 300 to 1500 meters to obtain photographic resolution more amenable to detailed interpretation of ice conditions and features. Low clouds (less than 150 meters) prevented RP-3A data collection on the 8 and 9 April tracks. Coincident data from the two aircraft were obtained on the 10, 11, and 12 April tracks. Areas of coincident SAR and RP-3A photographic data are shown in Figure 1. The 12 April CONVAIR-580 SAR track was flown on 13 April by the RP-3A aircraft. Ice deformation, which occurred during the approximate 24 hour period between these flights, is evident when comparing the coincident imagery.

GENERAL ICE CONDITIONS

The formation of ice in Baffin Bay generally begins in October. The early thin ice forms are easily broken into fragments of brash ice and ice cakes by wind and wave action. The fragments consolidate and both the deformational and consolidation processes may occur again and again. This interaction results in an icefield consisting of various sizes and shapes of ice fragments. Eventually, as the freezing process continues, a more stable consolidated ice cover is formed that has sufficient thickness to withstand wind and wave forces which easily deformed the ice earlier. In terms of surface roughness this ice cover will have a high density, but low relief. The fields of ice increase in size and extend southward into Davis Strait and over the Labrador Sea along the Canadian coast as the season progresses. The seaward edge of the ice, continually under the influence of sea and swell action, will remain broken and may be easily dispersed by winds and currents.

Deformation within the ice field continues throughout the season. The majority of newly formed ice in the fractures is deformed into ridges by shear stress and compression. Some areas, however, remain undisturbed and retain relatively smooth surfaces. Networks of pressure ridges and hummocks which form throughout the season are present in the ice. Ridges in this region are usually less than a meter high.

First-year ice and younger stages of ice development are the dominant sea ice types found in the eastern Canadian arctic region. Multi-year ice is not common in this area, although occasionally it is present. The multi-year floes have drifted into Baffin Bay from the Canadian Archipelago and Nares Strait. Icebergs, bergy bits, and growlers, derived primarily from Greenland glaciers, are common.

Air temperatures and the ice/snow surface temperatures in some of the experimental areas were above freezing prior to and during the experiment. Early surface melt conditions prevailed, producing slush or very wet snow, and some melt puddles.

SAR DATA

The SAR imagery is not calibrated, thus all inferences to radar backscatter are based on image gray tone differences, which may change from image to image. Many factors contribute to the relative backscatter (or gray tones) seen on the image from the time of system data collection through optical processing and, finally, during photographic processing procedures.

All four SAR channels were examined during this analysis. The imagery obtained from the cross-polarized channels was generally of poor quality, evidently lacking the dynamic range seen in the like-polarized channels. Minor differences noted between some frequency like- and cross-polarized imagery did not add to the quality of interpretation. With one exception (Figure 14), cross-polarized images are not illustrated.

Interpretation of the SAR imagery depended primarily on cross-correlation with the RP-3A 9-inch (24-cm) photography, and the accumulated experience and knowledge of the image analysts. The only ground truth information available

was from a few on-site observations obtained by the Danes in the Danish Experimental area southwest of Disko Island.

Once cross-correlations with photography have been made, interpretation of the SAR imagery is dependent on the interpretation of the sea ice photography. At times, this process becomes somewhat speculative, particularly in snow-covered areas or when key features affecting the radar return are not evident on the photograph. Additionally, it appears that some radar returns are not from the observed surface, but are from subsurface boundaries and/or volume scattering. Clearly, the history of the ice formation, deformation, decay, and current weather conditions determine the ice and snow surface and subsurface properties, including the distribution of dielectric properties. These factors, in turn, control the radar backscatter for a given set of radar equipment parameters. One very important question is: How transient are the properties of a given section of ice or snow relative to fluctuating weather conditions (i.e., changing air temperature, precipitation, blown snow, etc.)? The interpretations formulated during this analysis are presented with the understanding that, in future SAR experiments when ground truth is available, they can be either further developed or disproved.

SOUTHERN BAFFIN BAY DATA

This portion of the SURSAT experiment, initiated and planned by the Technical University of Denmark, was flown on 10 April 1979 over two predetermined crossing lines, one oriented north-south, one oriented east-west, located over ice fields southwest of Disko Island (see Figure 1). The experimental area included ice from the ice edge inward. Many small, thin cakes and floes derived from wave and swell broken floes dominated the area in the vicinity of the ice edge. Farther in from the edge, larger floes were dominant; some were a consolidation of small floes, others appeared to have developed under stable conditions and were more homogeneous in appearance and thickness. The majority of the sea ice was very thin first-year ice or young ice. Nilas was present and the presence of snow on the nilas surface indicated a recent snowfall. Nilas will not maintain a snow cover for long periods, especially with air temperatures (around -1°C) which existed during the experiment. The snow appeared thickest over the northwestern portion of the experimental area. Surface air temperatures the day before the flights were reported to be as high as + 4°C. Surface temperatures for snow, ice, and water during the flight were nearly isothermal, as indicated by the airborne radiation thermometer (PRT-5), averaging between 0°C and - 1°C. Evidence of earlier melting was observed. Helicopter landings and observations on two separate floes by Scott Polar Research Institute investigators on the morning of the experiment revealed a very wet snow about 10 cm deep, which covered ice about 20 cm thick. Ice conditions were too unstable for continued ground truth observations.

Analysis of the SAR imagery has strongly indicated that wet snow significantly increases X-band radar backscatter, but does not noticeably affect L-band radar backscatter. The processes of refreezing and recrystallization of moist snow could account for development of metamorphosed snow with the properties necessary to produce X-band radar return due to volume scattering.

Examples are shown in Figure 2, which displays X- and L-band SAR imagery from the east-west line, and Figures 3 and 4 which show some coincident photography taken from a 300-meter altitude at far range on the SAR imagery. The areas A and B in Figures 2 and 3 are areas of thin dark gray ice. Area A is covered with slush (saturated snow) that formed from recently deposited snow and displays either no or low X-band radar backscatter. Area B retains a great deal of snow cover which is in a state of deterioration. In both areas the ice surface is smooth. Area B gives a much brighter X-band radar return. The difference appears to be in the slush cover and melting snow cover. The far range portion of the L-band image shown does not display any information. However, areas A and B both appear as no return areas on earlier generation film strips. The rafted area between A and B provides some L-band return.

Figure 4 shows an area C of thin, smooth, snow-covered ice. Adjacent to area C is an area D of consolidated, snow-covered, smaller forms of different ages (breccia). The snow here is also undergoing melt. The X-band SAR imagery displays similar returns from the wet, snow-covered, smooth, thin ice C and from the breccia D. Although not readily apparent on the L-band image shown here, the rough-surfaced breccia D is giving a significant return, while the smooth, wet, snow-covered ice C is a no return area. These differences in the X- and L-band radar returns are critical to interpreting imagery taken during this equipment. The apparent high scattering cross-section of wet snow for X-band radar produces many ambiguous images. The L-band radar image, apparently unaffected by the wet snow, can be used to resolve the ambiguities, as one can see by comparing the upper portions of the X- and L-band radar images in Figure 2. Some of the brightest return areas on the X-band image appear dark on the L-band image. These areas are interpreted to be snow-covered thin ice that is similar to those areas of snow-covered thin ice shown on the photographs in Figures 3 and 4. Some areas in Figure 2 give returns on both channels. These areas are interpreted to be breccias or consolidated small forms similar to area D in Figure 4. Areas that are dark on both channels are inferred to be areas of open water or very thin ice without a snow cover. It is speculated that some of the variations in the gray tone pattern from the breccias on X-band radar may represent either structural variations in a recrystallized snow cover or variations in snow moisture content.

Areas of consolidated small ice forms and closely packed small ice forms are not well-discriminated by backscatter characteristics on either X- or L-band imagery, particularly at near range where image distortion is great and system resolution capabilities are reduced. The presence and distribution of small open or newly frozen areas may allow inference of unconsolidated conditions. SAR images illustrated in Figure 5 show a mixture of consolidated and closely packed small ice floes and cakes. A preponderance of both scattered thin ice (nilas) and open water areas exists over portions of this zone. The presence of consolidated forms of any significant size is unlikely in these areas. However, areas similar to that of A, although a nilas is evident, could be weakly consolidated and may include the nilas. The photographs in Figures 6 and 7 provide visual examples of ice conditions in this area. In comparing these photographs with the coincident SAR imagery, it is readily apparent that backscatter cannot be used to discriminate very closely packed small ice forms from consolidated small forms. In addition, only the snow-free areas of nilas, which appear as

low backscatter targets, can be discriminated as nilas on the X-band SAR image. The snow-covered dark gray ice has an X-band image tone and texture similar to the closely packed and consolidated thicker ice. L-band imagery better delineates all nilas-covered areas, since snow that is present apparently does not produce L-band backscatter. Note the apparent smaller size on the X-band radar image of the nilas-covered area at B (Figures 5 and 6). The snow cover around the periphery of this nilas-covered area produces X-band backscatter; thus, we see an apparent size difference of this target on the two channels. Another example of this difference is seen at A in Figure 5.

The open water area at C in Figure 5 provides no return signal on X-band imagery, but gives a return on L-band imagery. A similar phenomenon is shown on the radar image at D. This open water area is shown on the photograph in Figure 7. (The belt of small ice forms in the open water area moved there about one hour after the SAR imagery was collected.) In the L-band image in Figure 5 the open water area cannot be discriminated from the surrounding consolidated and very closely packed ice forms. This unusually high L-band return from open water was most common on the northern portion of the north-south line.

The photography indicated a recent snowfall, and it has been inferred from the photographic data that the snowfall was heavier in the northwestern portion of the experimental area. It is speculated that in areas of heavy snowfall, a fresh water-sea water mixture, which formed in the upper layer, provided scattering boundaries for L-band radar signals. Another interesting example of this anomalous L-band radar return is shown in Figure 8, which portrays ice conditions near the north end of the north-south line. Snow cover in this area, visible on the photographs shown in Figures 9 and 10, appears heavier than near the southern end of the line. Open water areas identified at A, B, C, and D (Figure 8) show no return on X-band imagery, but provide a good return on L-band imagery. The open water areas could be erroneously interpreted as ice cover on the L-band imagery. A photograph of Area A is shown in Figure 9. Several photographs of these areas of apparent open water, which produced high intensity L-band returns, were over-developed to see whether any ice could be detected. The results were negative.

The radar images shown in Figure 11 were taken along the southern portion of the north-south line. A number of no return open water areas are apparent on the X-band radar image. These areas also appear as no return areas on the L-band image, suggesting that a mixed water surface layer does not exist in this area or is not sufficient to produce L-band backscattering. Radar incidence angles are similar to those farther north where L-band backscatter was received from open water. The photographs in Figures 12 and 13 show some of the open water areas which appear at steep incidence angles on the SAR imagery (Figure 11). The surrounding ice does not have as much snow cover as observed on the ice farther north, i.e., less snowfall.

The examples already shown indicate that X-band radar backscatter is related to both ice surface roughness and snow conditions, whereas L-band radar returns are primarily related to the geometric shape and roughness of the ice surface (with the exception of the anomalous high returns from open water). The simultaneous use of both radars enables a more accurate evaluation of ice conditions, since L-band radar often can be used to resolve

ambiguities encountered on X-band imagery that are related to the high backscatter caused by a wet snow cover.

In some situations, the high X-band return related to snow can enhance interpretation of ice conditions; examples are shown on the 30 km long sections in Figure 14. These images were taken near the western end of the east-west line. The composition of some of the consolidated ice forms and their distribution is better depicted by the X-band imagery because of the high contrast between the ice fragments and the matrix ice which comprise the floes. For example, recent fragmentation of the thin first-year ice floes seen near the center of the strip is clearly indicated on the X-band images. This fragmentation is not discernable on the L-band image. The angular shapes (i.e. non-rounded edges of discrete fragments) of the fragments in the floes indicate that little deformation has occurred since the breaking apart of the original floe. Therefore, brash and block ice, which would normally present a rough ice surface geometry, are scarce in the matrix ice between the angular fragments, thus reducing the possibility of radar backscatter. As a result, there is little contrast between the matrix ice and the fragments on the L-band imagery. However, the X-band imagery shows a large backscatter difference between the matrix ice and the fragments. The high backscatter from the thin matrix ice is largely attributed to the snow cover. The left portion of the radar sections displays many floes composed of consolidated small, rounded forms of thin first-year ice. Again, small forms are better detected on the X-band imagery because of the difference in backscatter. The slightly better X-band radar resolution is also a factor. The deformed zones between the floes produce high returns with both radars, probably because of the brash and block ice which resulted from floe collisions. Snow in these zones enhances X-band return. The high returns from these deformed zones aid in the delineation of the floes. Many other areas in Figure 14 that display light tones on the X-band imagery, but dark tones on L-band, are areas of snow-covered thin ice. This difference is shown at several nilas-covered sites near the center and left portion of the strips.

The first-year ice and younger ice types dominating the area shown on the right portion of the radar images in Figure 14 do not appear to be weakly cemented consolidations of swell-fragmented ice as do the floes on the left portion of the images. The long linear character of many of the ridges in this zone supports this conclusion. Long, straight ridges in weakly cemented fragments of ice are uncommon. The imagery suggests that wave and swell action have played an important role in the deformation processes of the ice shown on the left end of the image strips, but not in the ice shown on the right end of the strips.

Generally, areas in this region showing low or no radar return on all three channels can be interpreted as areas of open water or thin ice with little or no snow cover. Areas which produce a substantial radar return on all channels have rough surface structure related to deformation. More tonal texture is usually apparent on the X-band image because of the shorter wavelength and slightly better resolution. High return X-band images with coincident low return L-band images are often related to snow-covered thin ice. The surface of this ice is generally smooth and the ice can be a thin first-year type. In areas having low X-band return but high L-band return,

penetration by the L-band signal is suspected with subsequent subsurface returns (Ketchum, 1978).

Some differences can be noted between the X_{HH} and X_{HV} imagery. It cannot always be determined if the differences in apparent backscatter are real or are due to variations in data processing techniques or dynamic range. For example, at areas marked A on the right end of the image strips in Figure 14, it appears that higher intensity returns were received on X_{HH} than on X_{HV}. In some cases the returns are more similar between L_{HH} and X_{HV} than between X_{HH} and X_{HV} (i.e., some areas having low L_{HH} returns also have low X_{HV} returns, but provide significant X_{HH} returns). These areas have been interpreted as smooth areas of first-year ice and evidently do not have the surface properties necessary for depolarization of the X-band signal. A more obvious distinction between the X_{HH} and X_{HV} imagery on the right end of the strips in Figure 14 is the greater clarity of the pressure ridge pattern on the X_{HV}. Background clutter reduces the ability to distinguish the ridges on the X_{HH} imagery. For the same reason, ridge identification is generally better on the L_{HH} than on the X_{HH} imagery.

In Figure 14 a number of icebergs, most of which are small, are tentatively identified because of their bright returns and shapes. However, all icebergs are not identified on all three channels and the quality of interpretation may vary with channels. The object at B is clearly shown by the X_{HH} radar, but is obscure on the X_{HV} radar and is not apparent on the L-band radar. There is some question as to whether this is an iceberg. The icebergs at C are identified on all three channels. The L-band image has no return areas within the icebergs. The largest iceberg on the imagery is shown at D. It is clearly depicted on the X-band channels, but again only a partial image is apparent on the L-band image. The distance between the two bright images, which are believed to represent the iceberg on L-band, is greater than the apparent length of the iceberg on the X-band imagery. The indication is that internal scattering of the L-band signal within the iceberg has caused a time delay, thus producing a false image which makes the iceberg appear either to be longer or as two icebergs.

EAST BAFFIN BAY DATA

Coincident SAR and photographic data collection was minimal. On 11 April, during the flight over Baffin Bay along the West Greenland coast (see Figure 1) from Sondrestrom AB to Thule AB, coincident data from the two aircraft were obtained at the beginning portions of passes 1 and 3. The ice conditions along pass 1 were very similar to ice conditions discussed above. Northward of pass 1, ice conditions changed from the breccia types and the fragmented conditions to more consolidated forms with an increase in ridging and in the number of icebergs. Surface temperatures along the northward run decreased progressively from -1.0°C to -8.0°C. It remains evident that snow conditions were still playing a dominant role in producing X-band radar backscatter, a backscatter which does much to reduce the ability to accurately interpret the sea ice conditions. As before, the use of the coincident L-band imagery resolves many of the ambiguities. Figure 15 shows a section of radar imagery taken at the beginning of Pass 3 on 11 April. Some coincident photography is shown in Figure 16. Some areas which are relatively smooth, but have a substantial snow cover, are marked A in Figures 15 and 16. These areas produce relatively low returns on the L-band image,

but relatively high returns on the X-band image. The high X-band return precludes discrimination of the more heavily ridged and hummocked areas on the X-band image, such as the ones marked B in Figures 15 and 16. The rough area B can be identified and delineated on the L-band image.

The iceberg at C in Figures 15 and 16 appears to provide a radar shadow on X-and L-band images. The shadow area is more distinct on the L-band imagery. The L-band imagery displays two bright images immediately below the iceberg. These images are believed to be time-delayed returns from the iceberg. Many icebergs exhibited this condition on the L-band imagery. Part of the radar shadow probably represents a period of no radar return during which the radar signals were "captured" within the iceberg. Lack of an anomalous signal in the space between the iceberg image and the false image seems to preclude consideration of volume scattering within the iceberg. This effect and the apparent high strength of the false image signals indicate multiple ice/water interface reflections within the iceberg and a focusing of energy on a reflective interface, which subsequently directed the signal back to the radar antenna. The approximate location of the false images on the terrain is shown on the photography in Figure 16. Other icebergs in Figure 15 also show false signals on the L-band imagery. The iceberg at D looks very similar on both the X- and L-band images, indicating that L-band returns, in this case, are directly from the iceberg as with X-band. However, a small image below the L-band iceberg image could represent a time-delayed signal. The iceberg at E is well-displayed on the X-band imagery, but on L-band imagery the area of the iceberg is represented by a shape similar to that shown on X-band, but has *no* backscatter with the exception of the small return area near the center. The iceberg at F is easily delineated on the X-band imagery, but on L-band imagery it is represented by five bright distinct scattered returns with little or no return between them. Even though the returns from the surrounding ice in the lower portion of the L-band imagery are suppressed, the iceberg returns appear to have saturated the radar. These returns are probably reinforced.

No correlative photographic data were obtained northward of the beginning portion of Pass 3 during the flight to Thule AB, Greenland, but earlier correlations have given interpretive clues when using coincident X- and L-band imagery in this area. To amplify, it has been hypothesized (Ketchum, 1977) that the development of the radar backscattering surface may be generated by the accumulation of environmental heat at the snow-ice interface. Salt or brine from within the ice migrates to this warmer zone and increases the salinity, thereby increasing the dielectric constant. Sufficiently high temperatures in this zone, due to trapped heat, cause metamorphosis of the ice and snow at their boundary and development of a recrystallized zone which is rough to X-band radar. The resulting combination of a radar rough surface and increased dielectric constant produces the radar backscattering surface. The amount of heat which accumulates at the snow-ice interface is primarily a function of ice thickness, snow thickness and density, air temperatures, and time.

Because of high return on the X-band image much of the thin ice bordering the new fracture is believed to have been recently snow-covered (Figure 17). Southerly winds, thought to be responsible for the most recent opening of the fracture, could have caused snow drifting onto the thin ice. Recent precipitation of snow may have occurred. The presence of thin ice on the

fracture is identified on L-band imagery only at the steeper angles of incidence. Areas interpreted to be mainly brash and block stand out clearly on L-band imagery. These areas are also high return areas on the X-band imagery, but are not as easily delineated due to background clutter. The wakes of brash and block associated with the differential motion of the sea ice and icebergs are also identified because of their high return on both channels. A false image is identified in association with the uppermost iceberg on the L-band image. As in Figure 15, some of the iceberg returns are very strong, indicating signal reinforcement.

Some backscatter variations observed on the X-band image in areas which show little return on the L-band image are believed to be due to variations in snow-ice interface development related to snow depth, ice thickness, and air temperatures. Minor variations in ice surface roughness may also be responsible for backscatter differences. However, a homogeneous gray tone indicates a very high density of scatterers, which tends to indicate an interface reflection.

Much of the ice cover shown on the radar images in Figure 18 is interpreted to be of fast ice origin. Both X- and L-band images display this ice with homogeneous high returns, which are attributed to a high density surface roughness related to the consolidation of many small fragments that formed during early growth of the fast ice. Ice fragmentation due to wave action is not uncommon because generally these areas are not protected by adjacent offshore ice fields during the early growth period of fast ice. The fast ice fragments are more pronounced and better delineated in the X-band image because the surrounding sea ice presents a much more variegated gray tone than in the L-band image, thus presenting more contrast in the pattern. The large areas of nilas adjacent to the fast ice fragments probably resulted from openings formed by differential motion of the thicker, heavier fast ice fragments and the surrounding drifting sea ice. Dark gray tones on the high return nilas in the lower portion of the X-band image appear to be flooded areas. Flooding would remove snow cover believed responsible for the high backscatter. The pattern orientation and extent of the indicated flooding could be related to the southerly winds which prevailed during this time. The dark lineations seen on the fast ice fragments are interpreted as thick ice frozen in the fractures which occurred while the ice was in its original shorefast location. The wider fracture is probably an old shear zone and the narrower fractures intersecting the shear zone may be tension fractures which developed during the shearing action. Friction caused by sea ice drifting adjacent to the fast ice zone was probably responsible for formation of the indicated shear zone. The initial orientation of the shear zone would then have closely paralleled the edge of the fast ice. Many icebergs are present in the lower left portion of the Figure 18 images. A false image is identified on the L-band image.

The X- and L-band radar image strips shown in Figures 19 and 20, respectively, were taken during a flight westward along the Greenland coast from Cape Melville to Cape York and beyond. Numerous icebergs, most rather small, are shown locked in the shorefast ice between Cape Melville and Cape York. The large concentration of icebergs immediately west of Cape Melville and east of Cape York indicate that this area is a primary source of icebergs in Baffin Bay. Icebergs are also seen in the drifting ice located west of Cape York. The sea ice adjacent to many of the icebergs exhibits low or no

radar return. Low radar return areas are also present on the sea ice along the coastline. No coincident photographic data are available to aid in identifying the nature of these low radar return areas. However, it is believed that the low return signatures may be related to the action of very strong winds from the Greenland ice cap and the resulting surface flooding. It is speculated that the flooding is directly related to the forces of the strong winds on the icebergs and sea ice surface.

Fracturing of the sea ice around the sea level bases of the icebergs and along the coastlines, due to wind forces, would provide the necessary openings for flooding. Snow removal and smoothing of the ice surface would result from the flooding process. Flooding is also present along cracks running between some of the icebergs in a direction normal to the strong winds. These cracks are probably related to the wind stress on the icebergs.

A dominant east-southeasterly wind over this area is indicated by snow drift pattern identified in association with the icebergs in the drift ice west of Cape York in the X-band imagery (Figure 19). The great length of the snow drifts suggests very strong winds. The shape and orientation of the low return areas in association with the icebergs and the coastline also suggest east-southeasterly winds. Although we do not have sufficient information to determine the processes involved, it appears fairly evident that very strong winds have played a significant role in the apparent fracturing and flooding process.

Many of the icebergs shown in the Figure 20 L-band imagery produced false images or images which represented time-delayed return signals. These icebergs generally showed less return than the same icebergs on the X-band imagery. In some cases lack of any backscatter indicates that all the radar energy has been lost through internal iceberg reflections.

Internal reflections are suggested by many low or no return areas shown on the L-band imagery of the ice-covered land masses in Figure 20. Many of these areas of reduced return on the L-band imagery and good returns on the X-band imagery (Figure 19) are interpreted to be glaciers or inland ice sheets. Further comparison of the coincident X- and L-band imagery may allow some determination of glacial ice distribution.

NORTH BAFFIN BAY DATA

Although the majority of ice in North Baffin Bay is first-year ice, it is comprised of various thicknesses, which are in different stages of development, and have experienced different degrees of deformation. Relative age identification, using aerial photography, is based primarily on visible surface roughness. The season's earliest ice formations may undergo considerable sea and swell action and other deformational activity before any semblance of stability is established in the ice cover as it grows thicker. Because of this more pronounced deformation in the early stages of ice growth, the surface layers may be comprised of many broken pieces which have been consolidated. The underlying layer of ice probably represents a more normal, homogeneous growth. This condition would suggest the presence of a rough boundary between an upper layer of deformed ice and a lower layer of

undeformed ice, a boundary which could act as a reflective interface if reached by microwave energy.

The 27 km long sections of coincident X_{HH} and L_{HH} SAR imagery in Figure 21, as with earlier dual frequency illustrations, show considerable backscatter variation in a single channel and significant backscatter variations from the same ice features on different channels. It has been stated that snow cover strongly affects backscatter and the backscatter variations seen in the X-band imagery. The L-band radar is not as strongly affected by snow cover, hence the frequent large variation in the display of the same ice features as imaged by the two channels. It is hypothesized that the variable X-band radar backscatter is due to the presence of moisture in the snow, the development of a reflective snow-ice interface (due to interactive processes dependent on various balances of ice thickness, snow depth and density, and air temperature), and the residual effects of melted, then refrozen, snow cover on a relatively thin ice surface. Examples of all these phenomena and their effects on X-band radar backscatter may be present in the Figure 21 radar image.

The radar imagery in Figure 21, which is correlated with the photograph in Figure 22, shows examples of radar backscatter; some of which can and some of which cannot be correlated with the variable surface roughness properties visible on the photography. The thinnest areas of first-year ice, some of which have been labeled A, have a thin snow cover over an apparently smooth ice surface with minor relief in the form of ridging and rafting. On the X-band imagery, these areas cannot be readily distinguished from the areas labeled B which are areas of thicker first-year ice with ridging and consolidated fragments and an apparent deeper snow cover. However, since the backscatter from these visibly different areas of surface roughness is very similar, the primary backscatter is believed to be related to a weakly developed snow ice interface on both ice types, not to the deformational features.

The L-band radar appears unaffected by a snow-ice interface development on the thin, smooth first-year ice areas A and displays low or no radar return. The thicker, rougher first-year ice areas B show a higher return than that displayed on the X-band imagery. This comparison suggests penetration and subsurface backscatter of the L-band radar signals. The interface of a two-layer ice cover suggested earlier (consolidated pieces of deformed ice in the upper layer overlying a more normal homogeneous lower layer) may be the reflective boundary for this suggested subsurface return. Areas labeled C have extremely rough surfaces (high density of rubble and ridges) and provide returns at both radar wavelengths. On the L-band imagery these high return areas cannot be readily distinguished from the high-return B areas, again suggesting that visible surface roughness does not play the primary backscattering role with the L-band radar. The high X-band returns from the C areas seem to be more closely related to surface roughness, but again a snow-ice interface development within the heavily deformed areas could make an important contribution to the backscattering. The ice conditions shown by the photograph in Figure 22 probably closely represent ice conditions throughout the left portion of the radar strips shown in Figure 21. It is clear that the smooth, thin, first-year ice areas can be readily identified only on the L-band imagery, and that identification of the

extremely rough areas can be done with more confidence, although subjectively, using the X-band imagery.

The center portion of the SAR images shown in Figure 21 has a less intricate pattern of gray tones than the imagery shown on the left and right ends of the radar sections. This difference is greater on the X-band imagery because of the greater X-band radar sensitivity to surface conditions, particularly the suggested snow effects and snow-ice interface conditions. The center portion of the imagery does not depict much ridging, but the homogeneous high X-band returns, which indicate a high density of backscatterers (as would be expected from a reflective snow-ice interface) do much to obscure or mask returns from the ridges which are present. On the L-band imagery there is also a high, homogeneous return that may obscure ridge identification. The small size of many of the ridges and steep antenna angles may be factors here, too. The high L-band returns, which are homogeneous throughout this area, are attributed to subsurface reflections. It is apparent that reflective properties not discernible on the photography (Figure 23) are responsible for much of the radar return imaged by both X-band and L-band and that the masking effect of these "anomalous" returns reduces the ability to accurately interpret the sea ice conditions, particularly with respect to surface topography. As with the coincident SAR imagery and photography shown in Figures 21 and 22, respectively, areas identified as thin, smooth first-year ice A and rougher, thicker first-year ice B appear to be similar on the X-band imagery, but different on the L-band imagery. On X-band imagery, areas of greater surface roughness C provide the highest radar return, but on L-band imagery the extremely rough areas C cannot be easily distinguished from much less rough first-year ice B because of the similar returns. The thin, smooth, first-year ice at A is easily distinguishable on the L-band imagery by the low contrasting returns. The thin ice-covered fracture shown by the coincident SAR imagery and photography in Figures 21 and 23, respectively, gives a high X-band, but low L-band radar return. The 5000-foot altitude photography, which was taken about 24 hours after the SAR imagery, does not readily reveal a snow cover on the thin ice, but close examination of the photography reveals areas of flooding associated with recent rafting. The flooding has left darker surface areas on the photography and low radar return areas on the X-band imagery. It is evident that flooding has removed a portion of the surface material, probably snow cover or some residue from a former snow cover, and that this material had the properties necessary to produce X-band radar backscatter.

Ridge detection on the data examined during the analysis has been difficult in many areas. Many ridges do not produce discernible radar returns. This may, in part, be due to small ridge size in terms of the radar resolution and steep antenna angles; however, background clutter obscuring ridge detection seems to be the principal reason. It is evident, when comparing the photograph in Figure 24 with the SAR images in Figure 21, that the most outstanding high return features on the X-band imagery are snow-covered, thin-ice-filled narrow fractures. These areas, some of which are labeled A, Figure 21, are often found in association with and parallel to, or within a ridged area. These areas may be accidently overlooked visually because of snow cover. The relatively large ridge at B in Figure 21, is delineated on both channels. Portions of this ridge are relatively new, as affirmed by the lack of snow drifts. Recent flooding adjacent to the ridge, with associated snow and ice changes as well as the recently frozen

snow-covered fracture parallel to this ridge, probably accounts for the radar return. Delineation of ridges on the right end of the radar section in Figure 21 is generally better than for the rest of this section; reduced background clutter is one reason. Discrimination of ridges from narrow ice-covered fractures could be difficult. The often sinuous nature of ridges, as compared to fractures, may sometimes be the best clue for interpretation. The newly opened fractures, depicted on the photography, were not present about 24 hours earlier when the SAR imagery was taken. The new fracturing, along the lines of the earlier fracturing, may have been underway. It seems implicit in this SAR imagery, as with the SAR imagery farther south, that in some way changes in snow properties have a profound effect on X-band radar backscatter.

CONCLUSIONS AND DISCUSSION

This analysis has clearly indicated the usefulness of dual-frequency SAR imagery to increase the objectivity of sea ice imagery interpretation, particularly in the marginal seas or areas which have large concentrations of relatively thin ice, a high incidence of snow, and large fluctuations in air temperatures. Combinations of these factors seem to contribute to changes in snow properties and to the development of a snow-ice interface, both of which appear to play important roles in X-band radar return. These observed phenomena produce many ambiguities in interpretation of X-band radar imagery; but coincident L-band radar imagery, which is not noticeably affected by these phenomena, can often be used to resolve these ambiguities.

Penetration of sea ice by the long wavelength L-band radar is not uncommon and subsurface returns are suspected. Hence, L-band radar as well as X-band radar imagery may, at times, be a poor indicator of ice surface topography when the masking effect of background clutter dominates the scene. In general, discrimination of various stages of growth and deformation of first-year ice was often very subjective with the X- and L-band radar imagery used during this analysis. Ice pressure ridge identification and discrimination were often poor and sometimes could not be carried out. Both deficiencies have been largely attributed to background clutter (snow and snow-ice interface backscattering with X-band, and subsurface backscattering with L-band).

Small ice ridge sizes versus the system resolution and the steep antenna angle also may be reasons for not discerning more ridges. The false images or time delayed L-band signals from icebergs were seen for the first time in this analysis. This prima facie evidence demonstrates that icebergs are penetrated by L-band radar. The illustrated variations of this effect (and lack of it) suggest that the internal structure and composition of icebergs vary considerably. Based on the evidence presented in this analysis, it is suggested that a comparative evaluation of coincident X- and L-band radar imagery of glaciated areas may lead to some assessment of glacial ice distribution over land masses.

BIBLIOGRAPHY

INTERA Environmental Consultants, Ltd. (1978). SAR 580 Production System. INTERA Report ASP-78-8, Aug.

Janza, Frank J., ed. (1975). Manual of Remote Sensing, V. I., Theory, Instruments and Techniques. American Society of Photogrammetry.

Ketchum, R.D., Jr. (1977). An Evaluation of Side Looking Radar Imagery of Sea Ice Features and Conditions in the Lincoln Sea, Nares Strait, and Baffin Bay. NORDA Technical Note 7.

Ketchum, R.D., Jr. (1978). An Evaluation of ERIM X-L Band Airborne Synthetic Aperture Radar Imagery of Sea Ice. NORDA Technical Note 28.

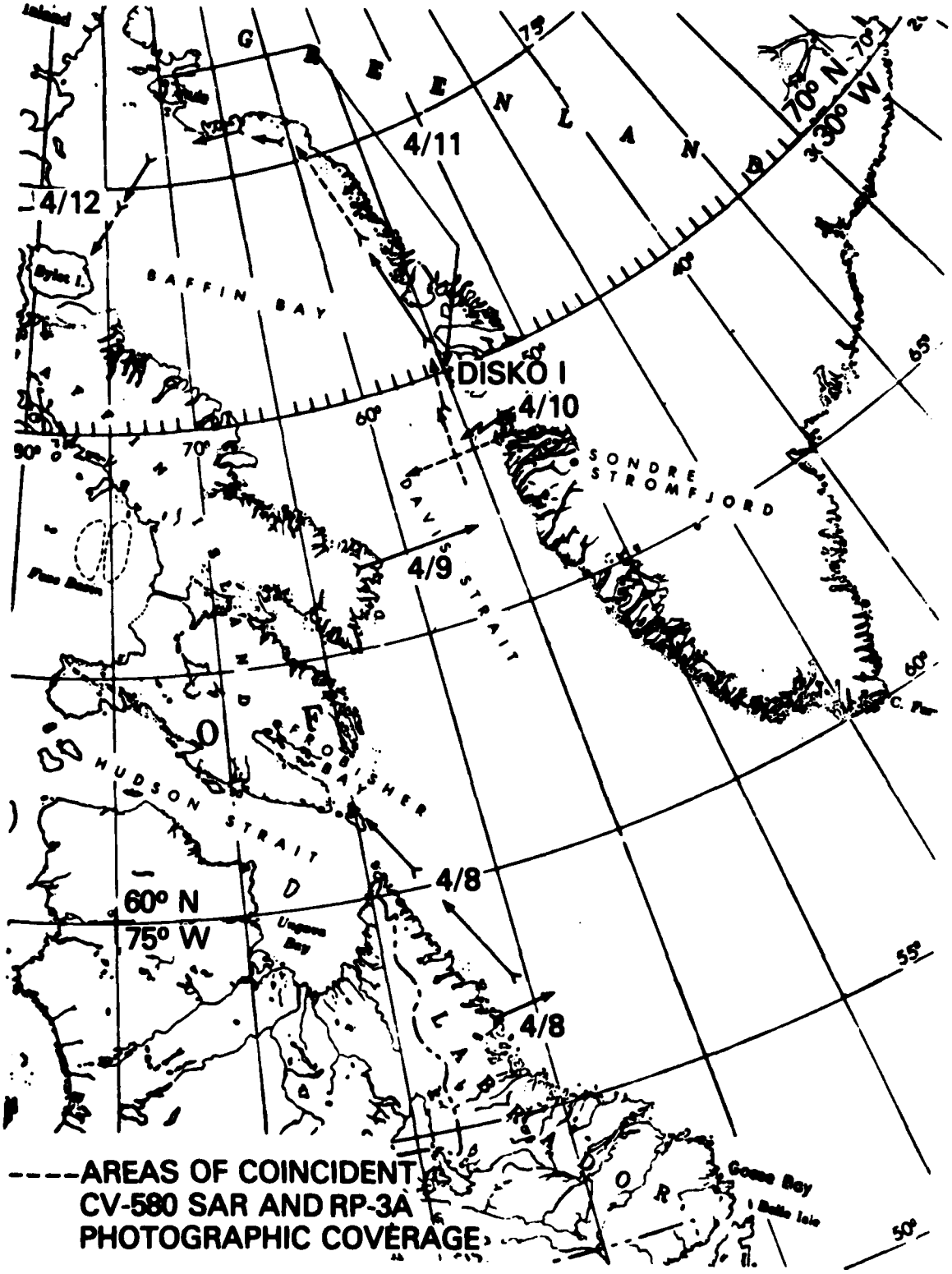

----AREAS OF COINCIDENT CV-580 SAR AND RP-3A PHOTOGRAPHIC COVERAGE

FIGURE 1. SURSAT CV-580 AND RP-3A FLIGHT TRACKS IN EASTERN ARCTIC,APRIL/1979

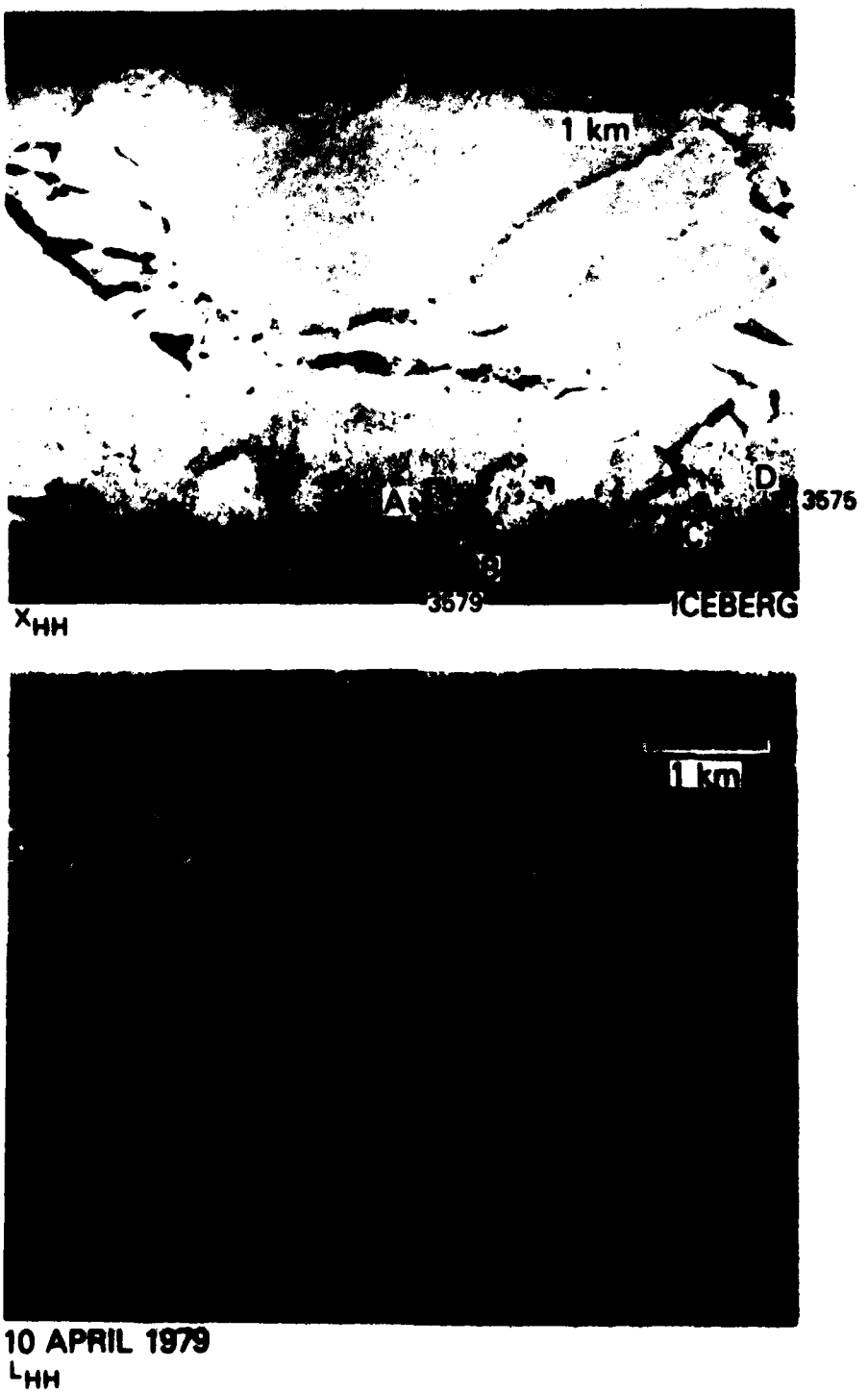

FIGURE 2 COINCIDENT X_{HH} AND L_{HH} SEA ICE SAR IMAGES TAKEN IN DAVIS STRAIT, 10 APRIL 1979.

FIGURE 3 AERIAL PHOTOGRAPH (305 M ALTITUDE) TAKEN IN DAVIS STRAIT, 10 APRIL 1979. CORRELATES WITH FIGURE 2 SAR IMAGERY.

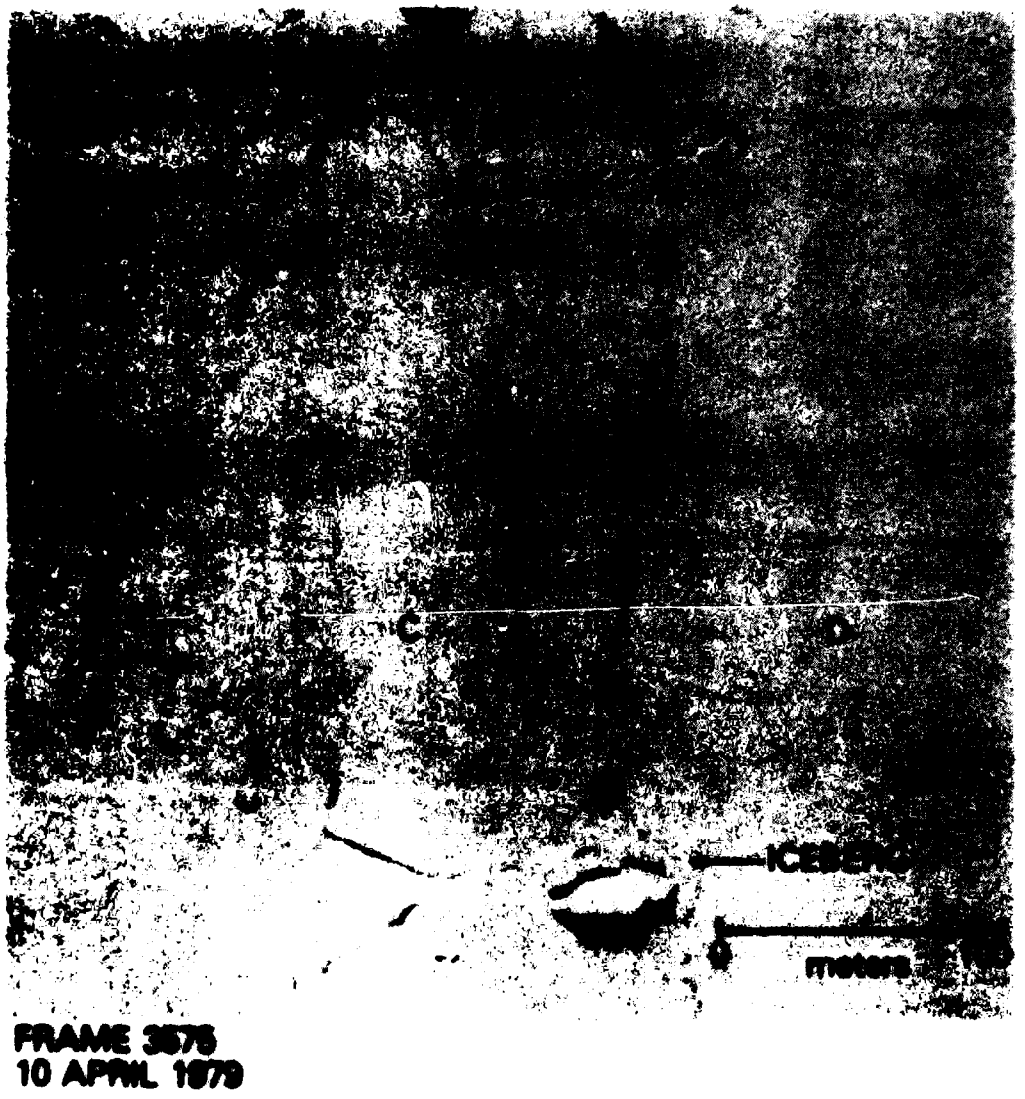

FIGURE 4 AERIAL PHOTOGRAPH (305M ALTITUDE) TAKEN IN DAVIS STRAIT, 10 APRIL 1979. CORRELATES WITH FIGURE 2 SAR IMAGERY.

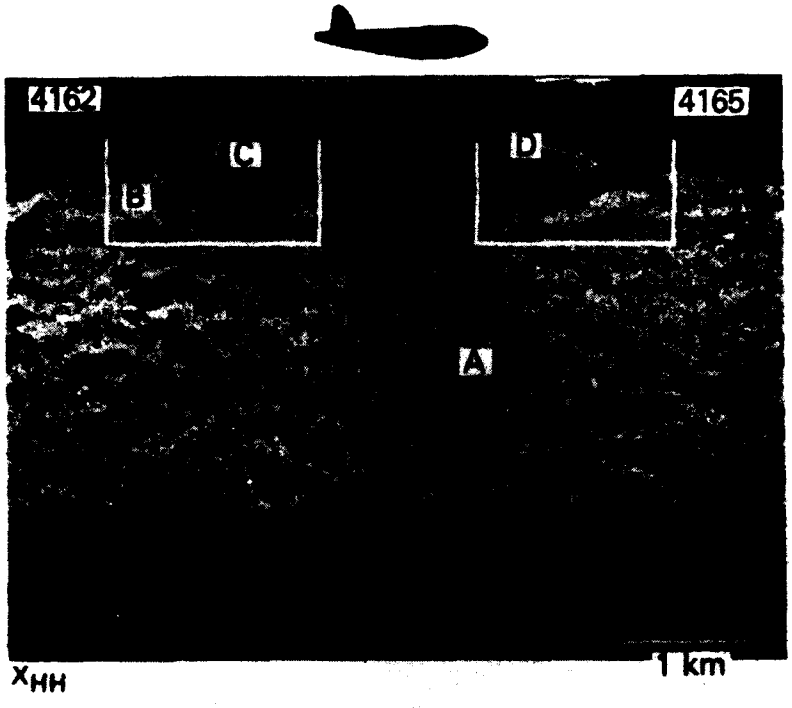

FIGURE 5 COINCIDENT X_{HH} AND L_{HH} SEA ICE SAR IMAGERY TAKEN IN DAVIS STRAIT, 10 APRIL 1979.

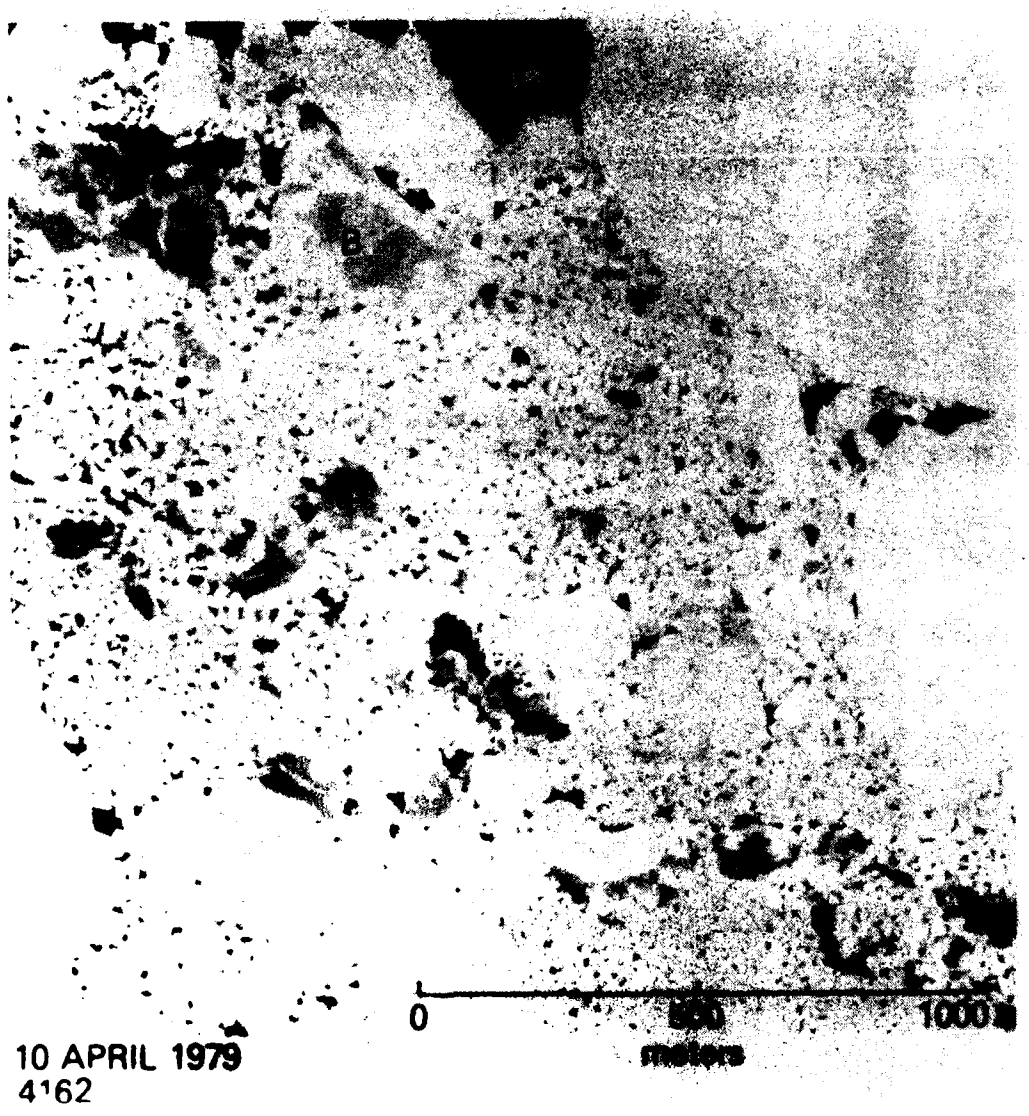

FIGURE 6 AERIAL PHOTOGRAPH (1524M ALTITUDE) TAKEN IN DAVIS STRAIT, 10 APRIL 1979. CORRELATES WITH FIGURE 5 SAR IMAGERY.

FIGURE 7 AERIAL PHOTOGRAPH (1524M ALTITUDE) TAKEN IN DAVIS STRAIT, 10 APRIL 1979. CORRELATES WITH FIGURE 5 SAR IMAGERY.

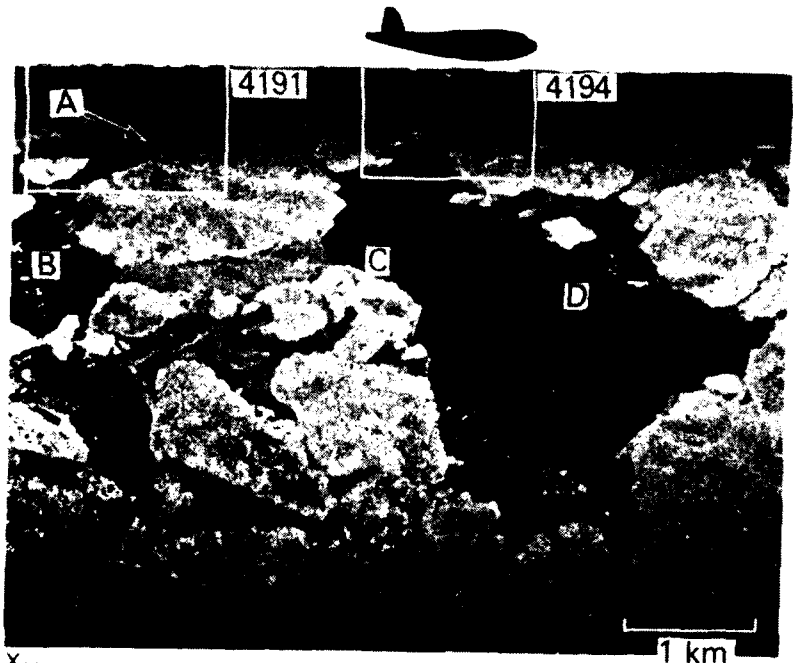

X_{HH}

10 APRIL 1979

L_{HH}

FIGURE 8 COINCIDENT X_{HH} AND L_{HH} SEA ICE SAR IMAGERY TAKEN IN DAVIS STRAIT, 10 APRIL 1979.

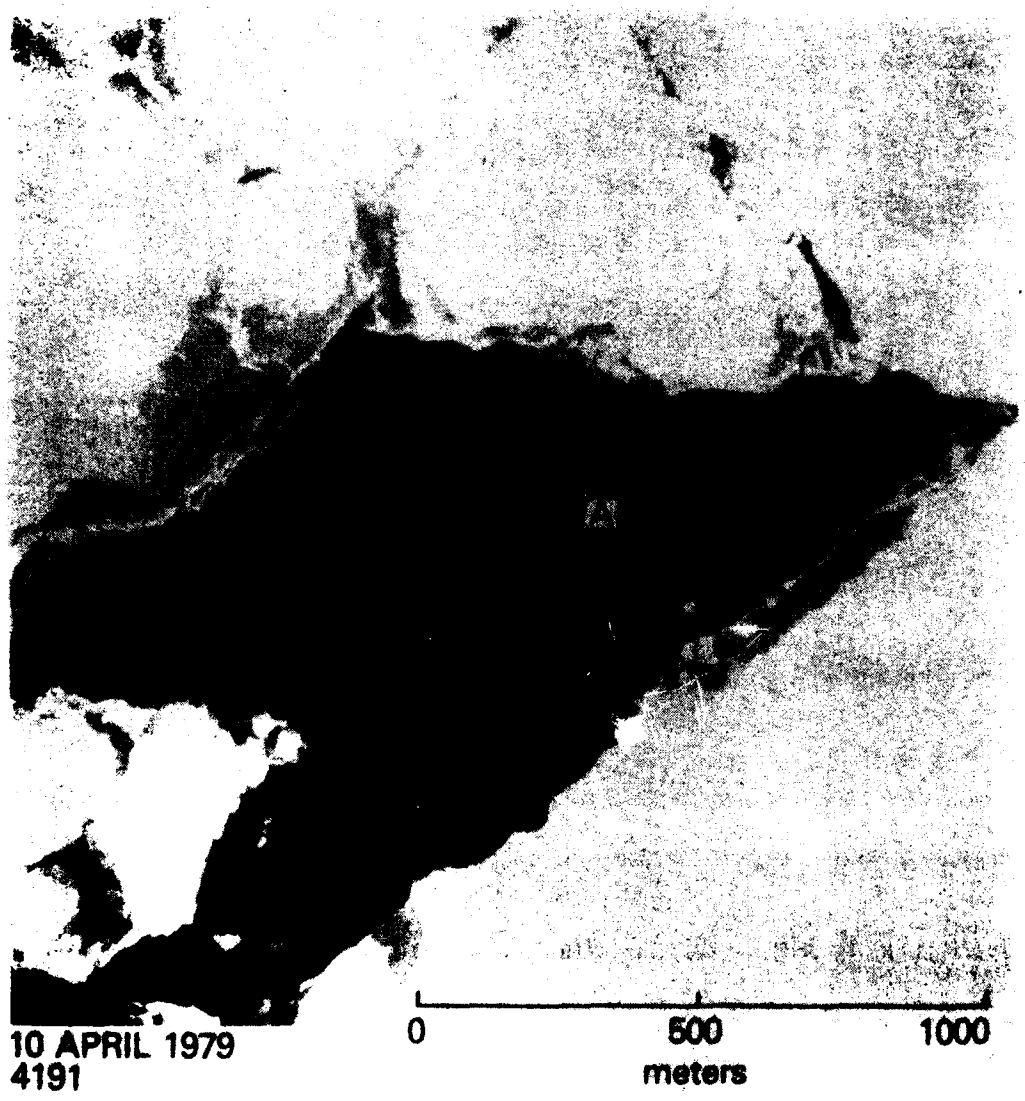

FIGURE 9 AERIAL PHOTOGRAPH (1524M ALTITUDE) TAKEN IN DAVIS STRAIT, 10 APRIL 1979. CORRELATES WITH FIGURE 8 SAR IMAGERY.

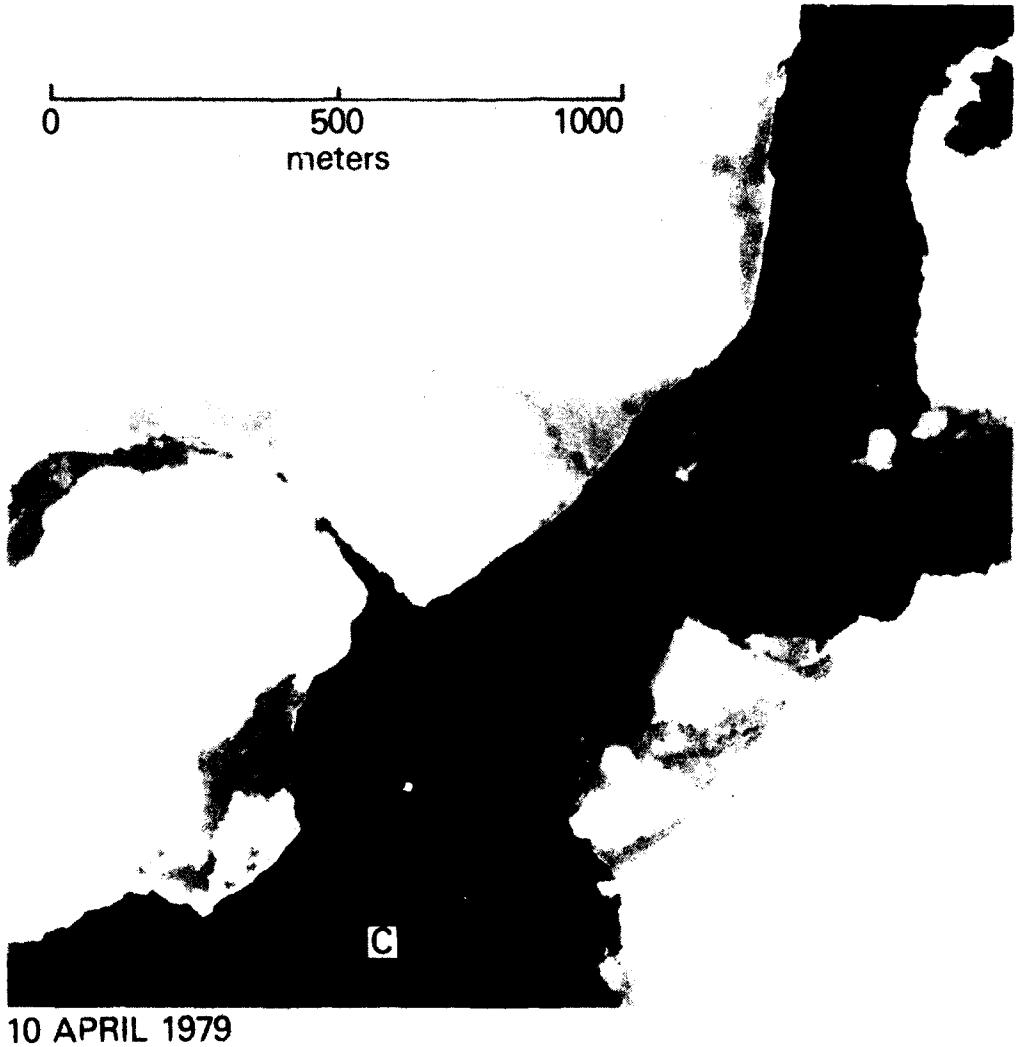

FIGURE 10 AERIAL PHOTOGRAPH (1524M ALTITUDE) TAKEN IN DAVIS STRAIT, 10 APRIL 1979. CORRELATES WITH FIGURE 8 SAR IMAGERY.

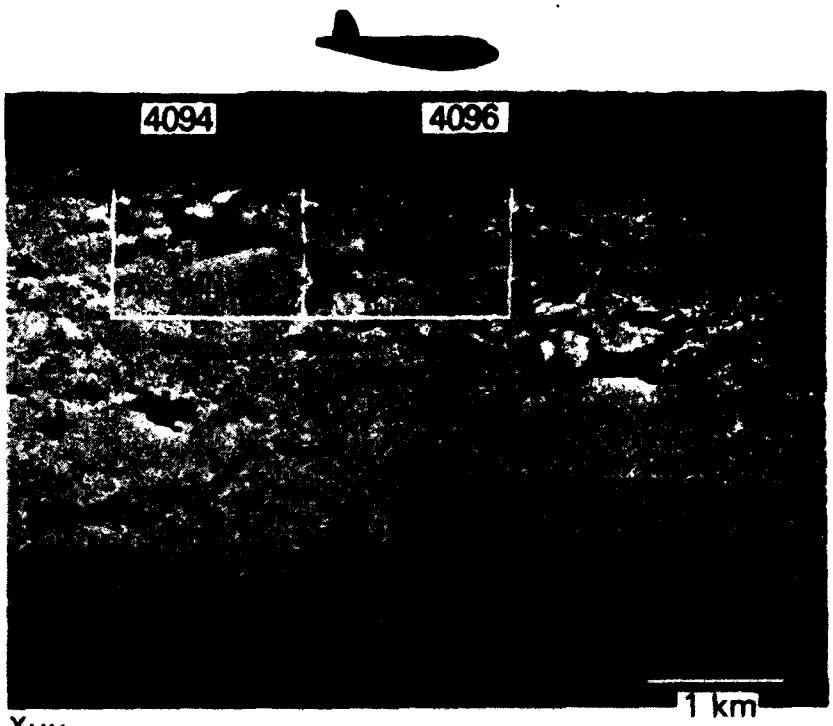

X_{HH}

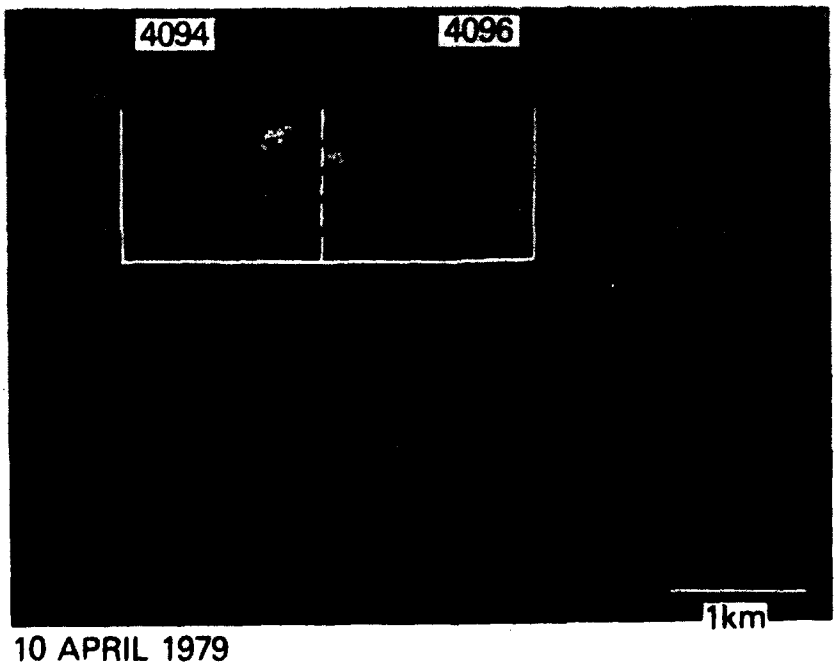

10 APRIL 1979

L_{HH}

FIGURE 11 COINCIDENT X_{HH} AND L_{HH} SEA ICE SAR IMAGERY TAKE IN DAVIS STRAIT, 10 APRIL 1979.

FIGURE 12 AERIAL PHOTOGRAPH (1524M ALTITUDE) TAKEN IN DAVIS STRAIT, 10 APRIL 1979. CORRELATES WITH FIGURE 11 SAR IMAGERY.

FIGURE 13 AERIAL PHOTOGRAPH (1524M ALTITUDE) TAKEN IN DAVIS STRAIT, 10 APRIL 1979. CORRELATES WITH FIGURE 11 SAR IMAGERY.

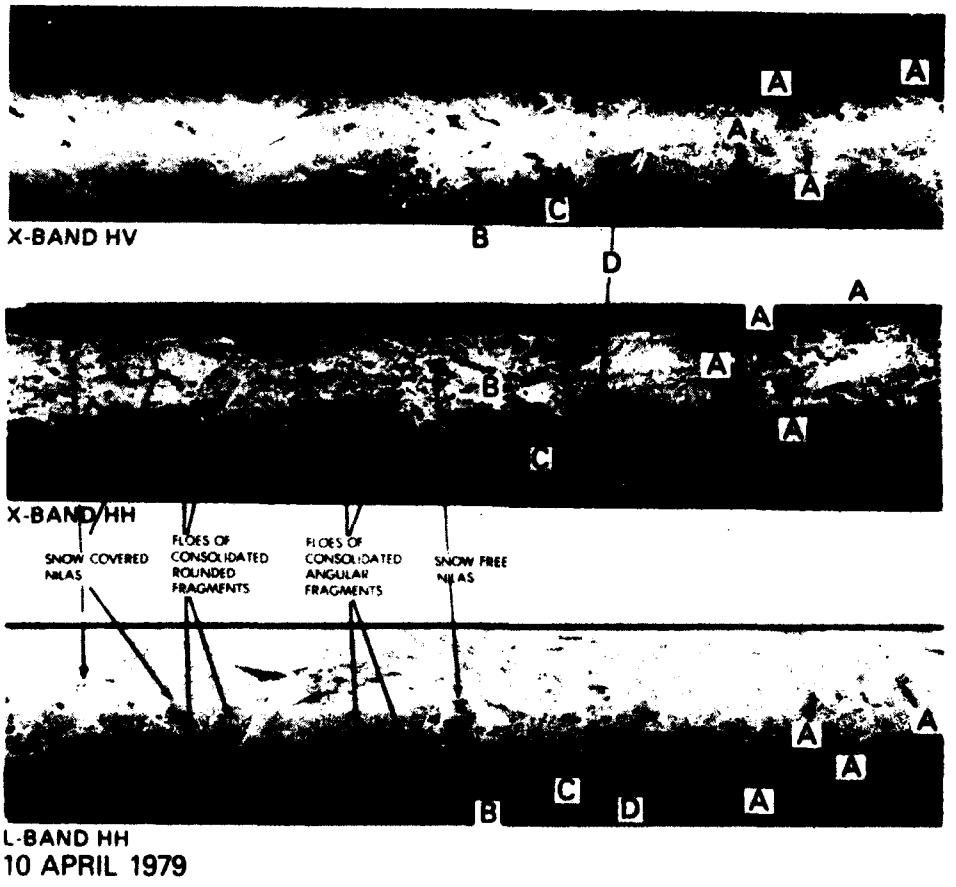

FIGURE 14 COINCIDENT X_{HH} AND L_{HH} SEA ICE SAR IMAGERY TAKEN IN DAVIS STRAIT, 10 APRIL 1979.

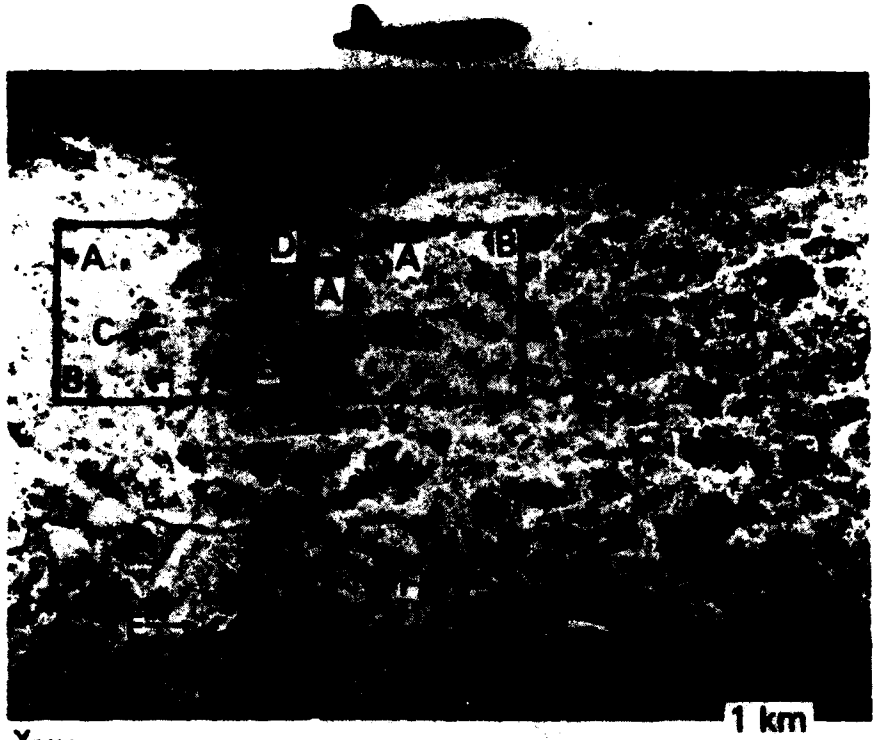

X_{HH}

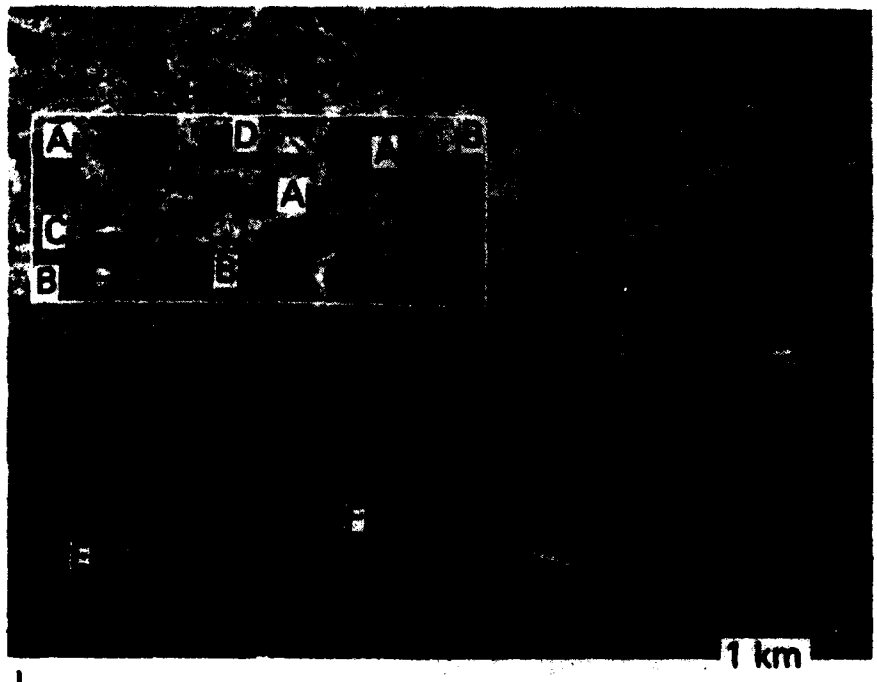

L_{HH}

11 APRIL 1979

FIGURE 15 COINCIDENT X_{HH} AND L_{HH} SEA ICE SAR IMAGERY TAKEN IN BAFFIN BAY, 11 APRIL 1979.

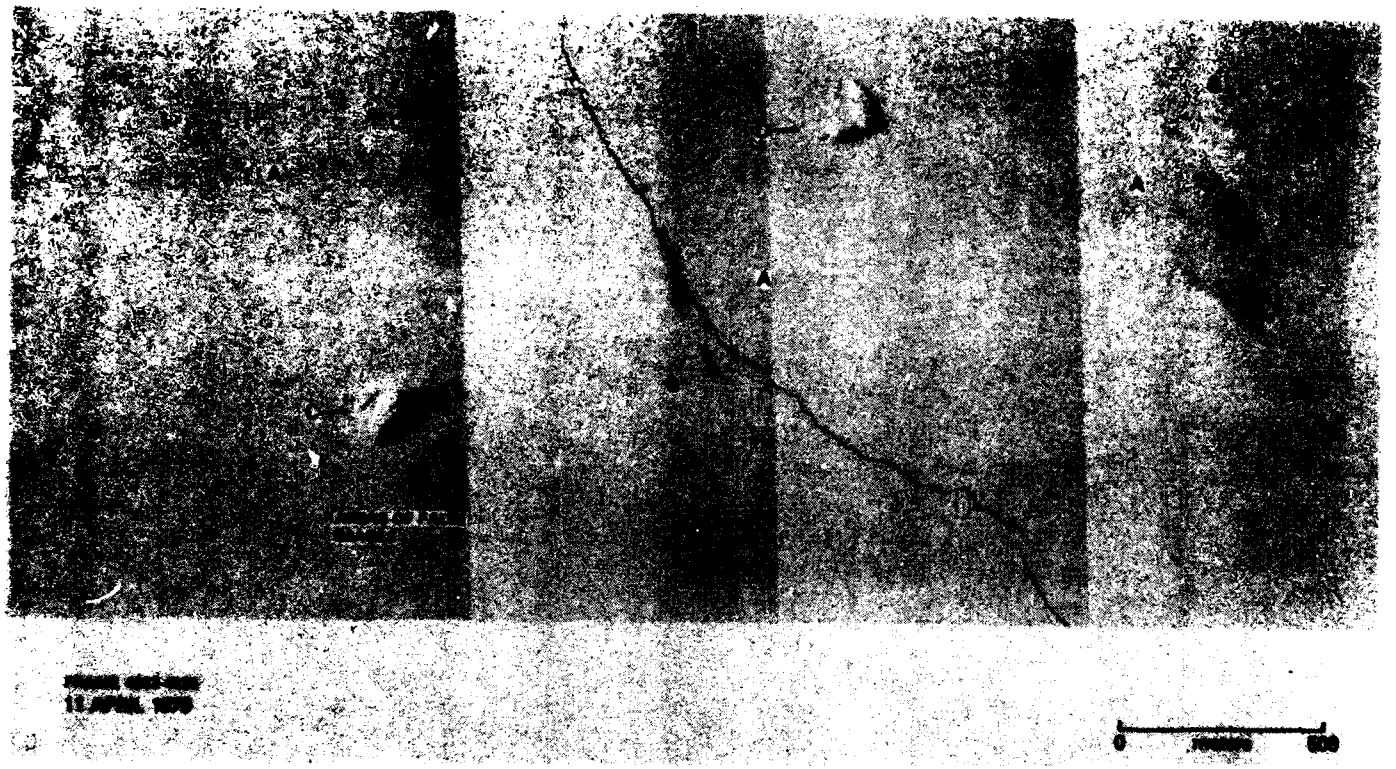

FIGURE 16 AERIAL PHOTOGRAPHY (1524M ALTITUDE) TAKEN IN BAFFIN BAY, 11 APRIL 1979. CORRELATES WITH FIGURE 15 SAR IMAGERY.

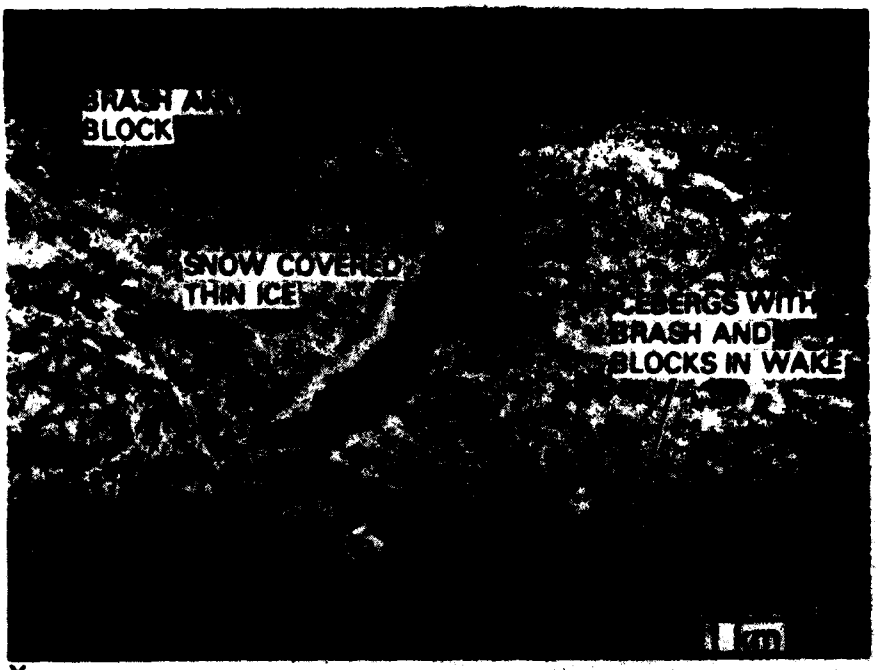

X_{HH}

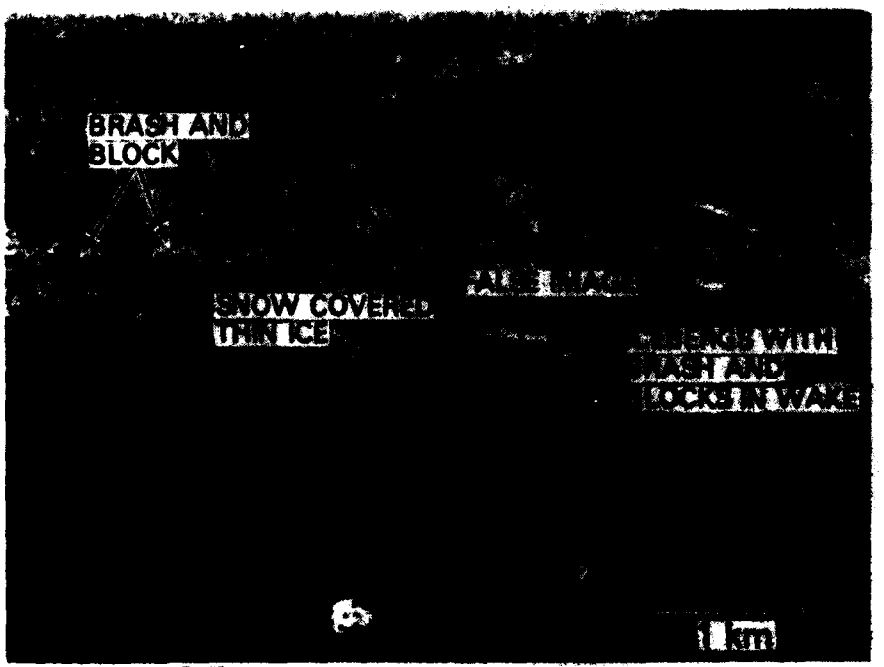

11 APRIL 1979
L_{HH}

FIGURE 17 COINCIDENT X_{HH} AND L_{HH} SEA ICE SAR IMAGERY TAKEN IN BAFFIN BAY, 11 APRIL 1979.

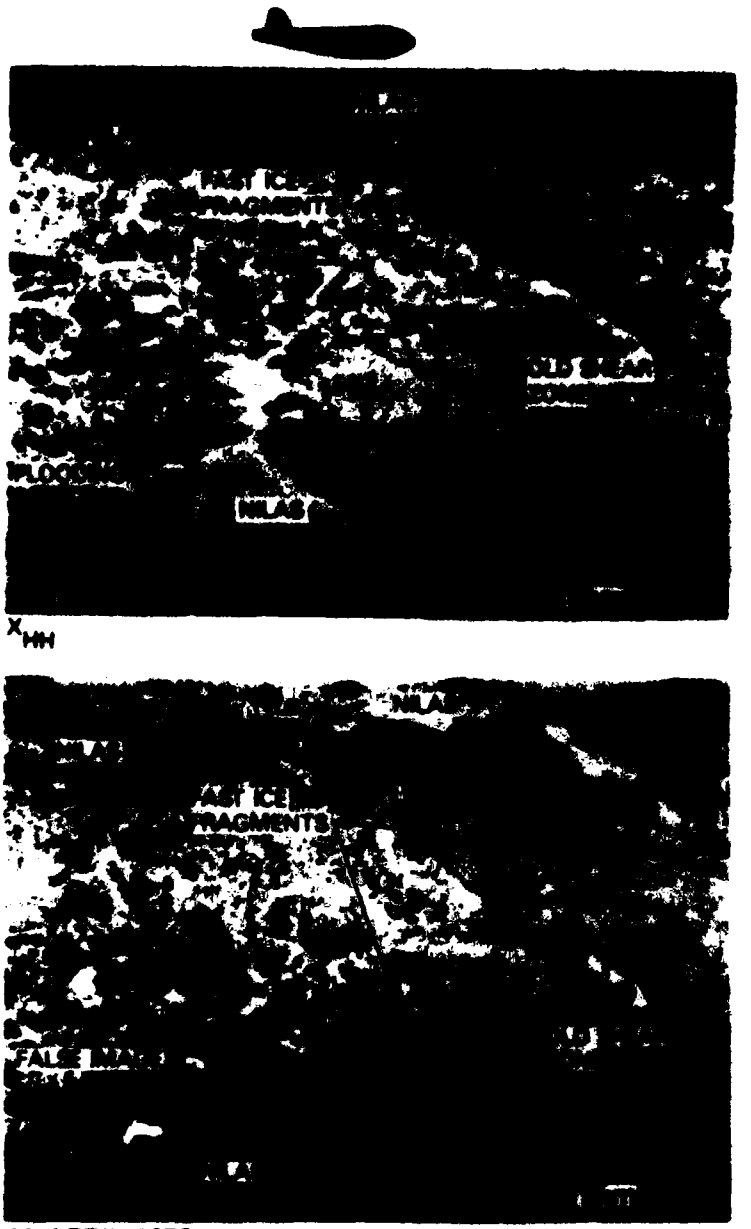

FIGURE 18 COINCIDENT X_{HH} AND L_{HH} SEA ICE SAR IMAGERY TAKEN IN BAFFIN BAY, 11 APRIL 1979.

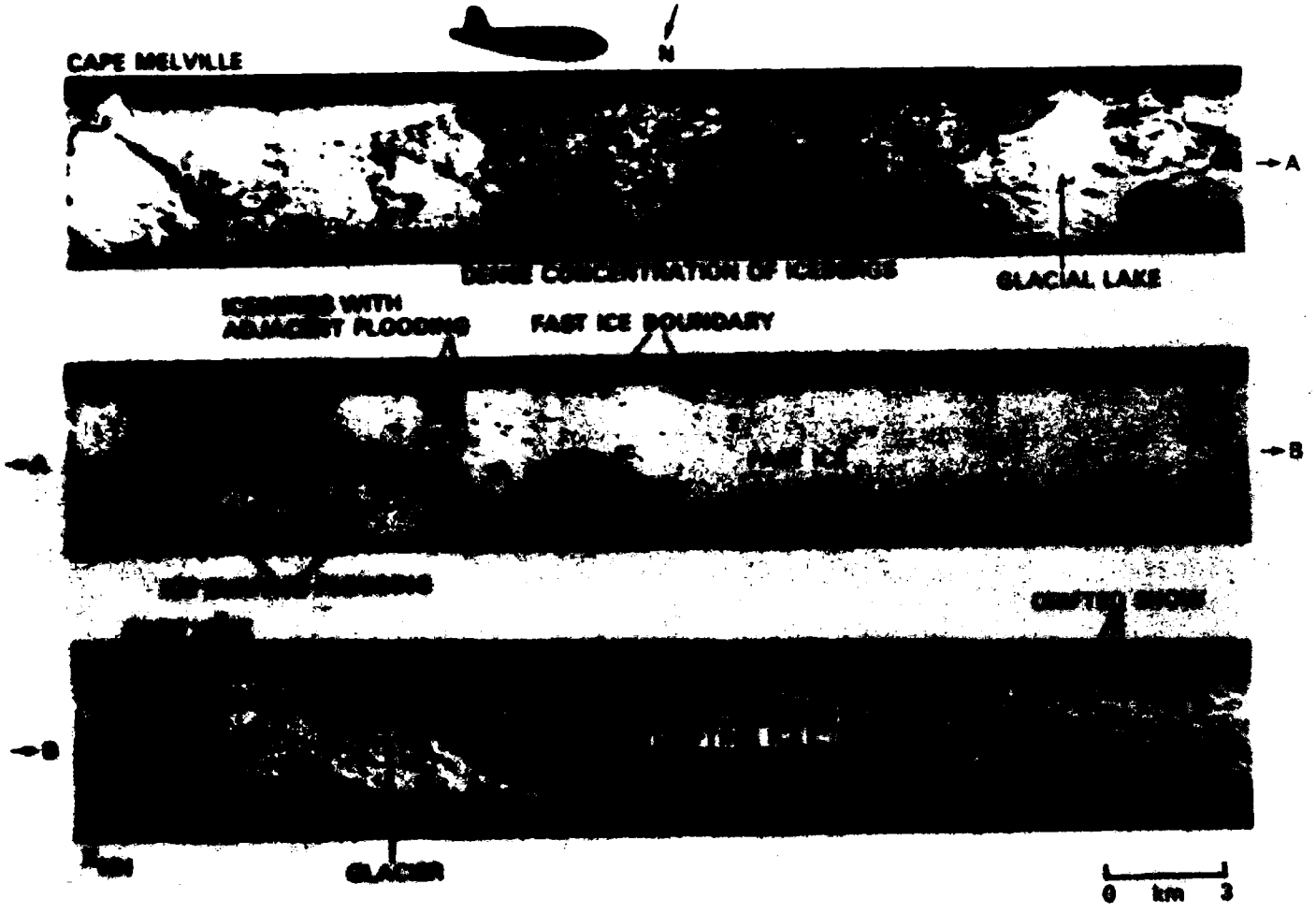

FIGURE 19 X_{HH} SEA ICE SAR IMAGERY TAKEN IN BAFFIN BAY, 11 APRIL 1979. CORRELATES WITH FIGURE 20 SAR IMAGERY.

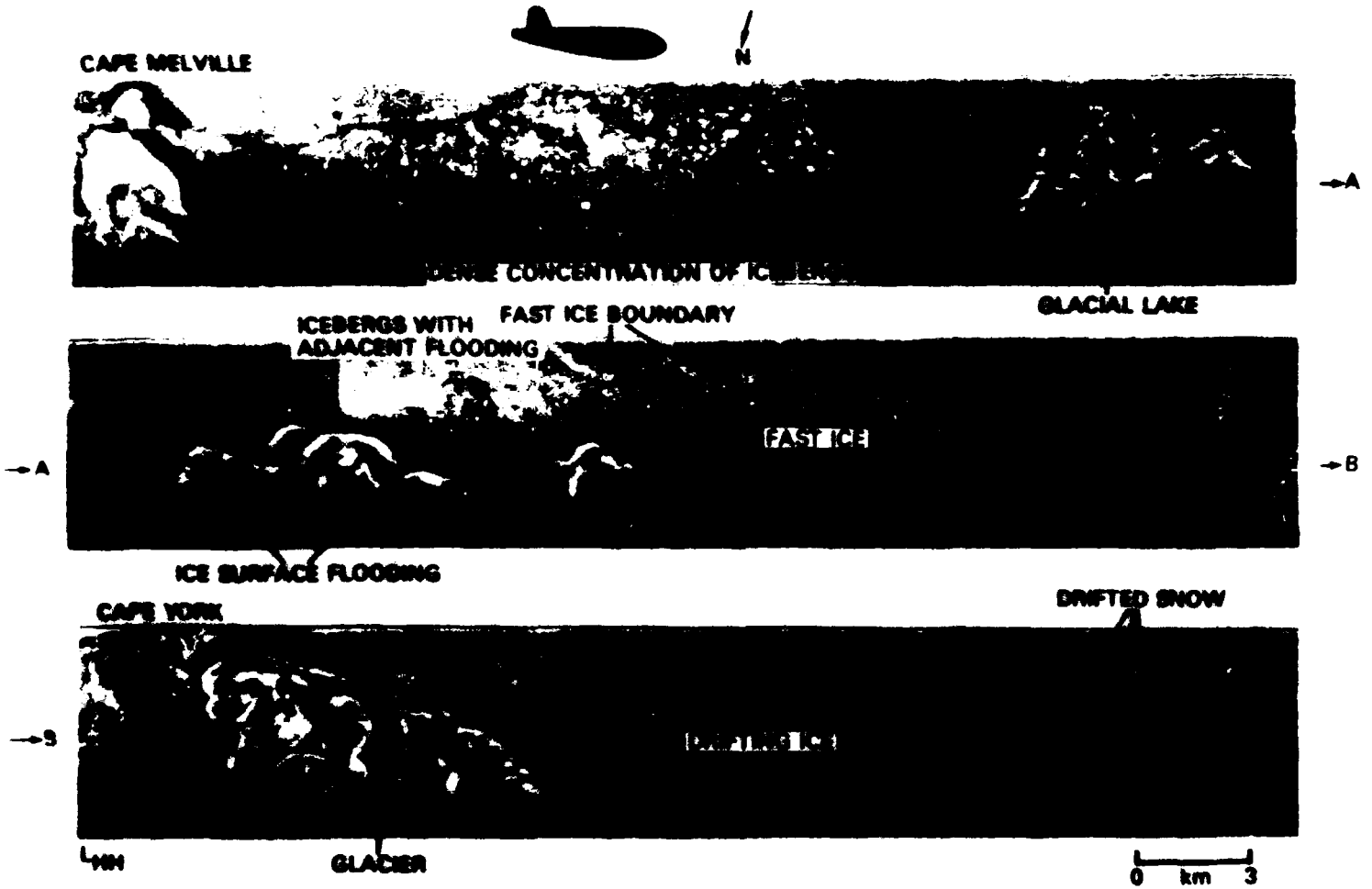

FIGURE 20 LHH SEA ICE SAR IMAGERY TAKEN IN BAFFIN BAY, 11 APRIL 1979. CORRELATES WITH FIGURE 19 SAR IMAGERY.

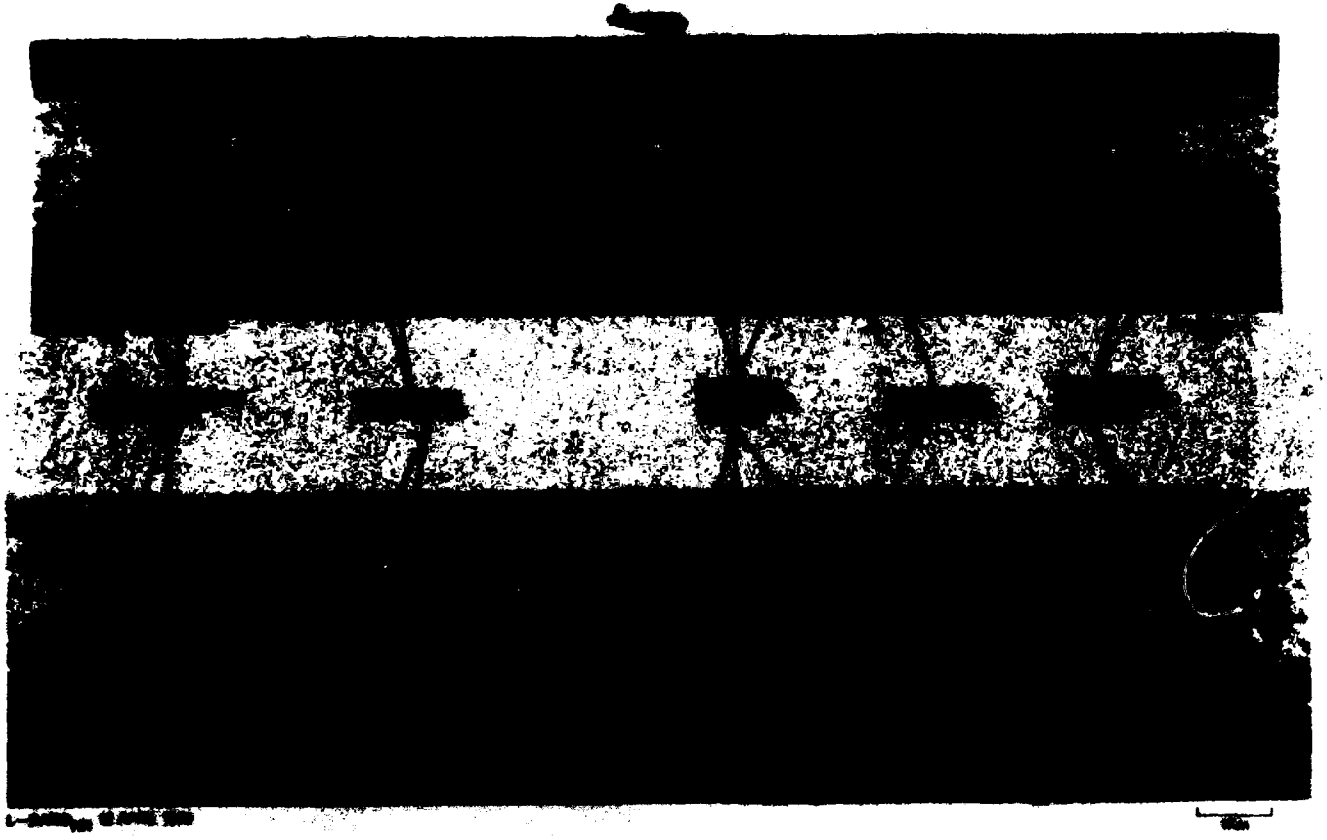

FIGURE 21 COINCIDENT X_{HH} AND L_{HH} SEA ICE SAR IMAGERY TAKEN IN BAFFIN BAY, 12 APRIL 1979.

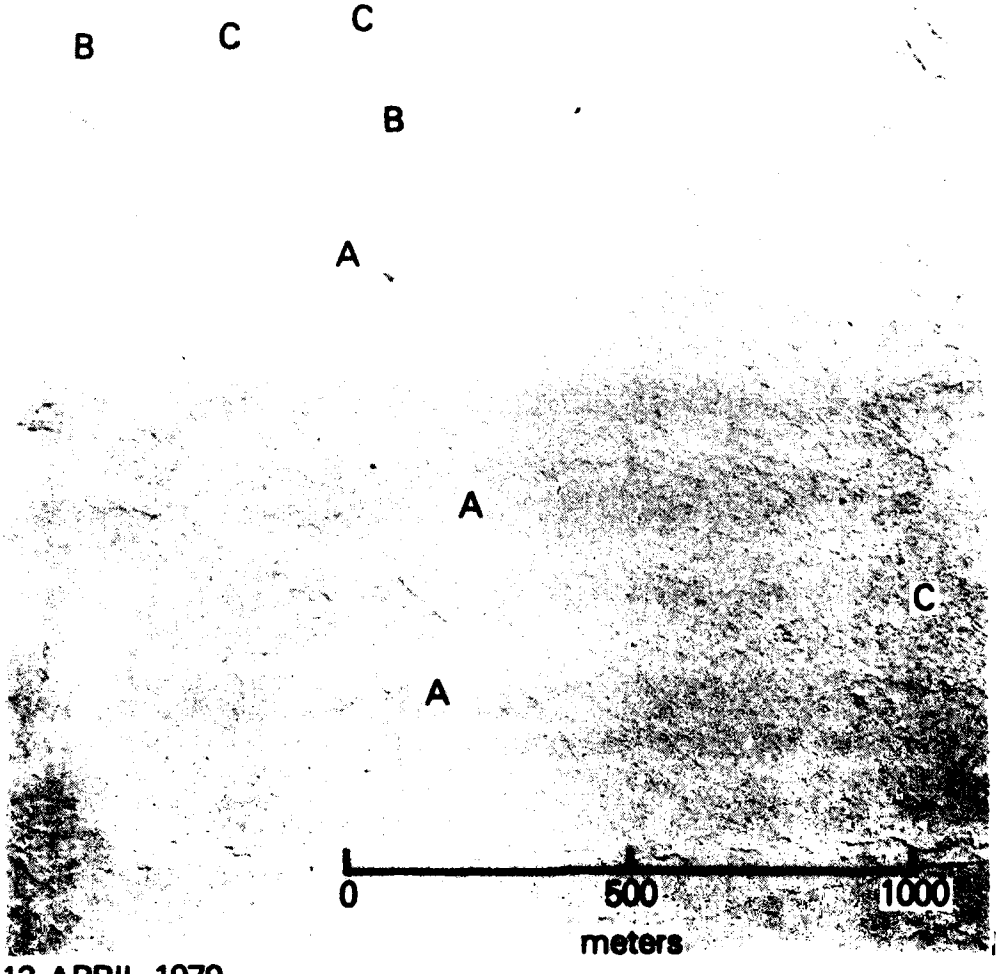

13 APRIL 1979
FRAME 5256

FIGURE 22 AERIAL PHOTOGRAPH (1524M ALTITUDE) TAKEN IN BAFFIN BAY, 13 APRIL 1979. CORRELATES WITH FIGURE 21 SAR IMAGERY.

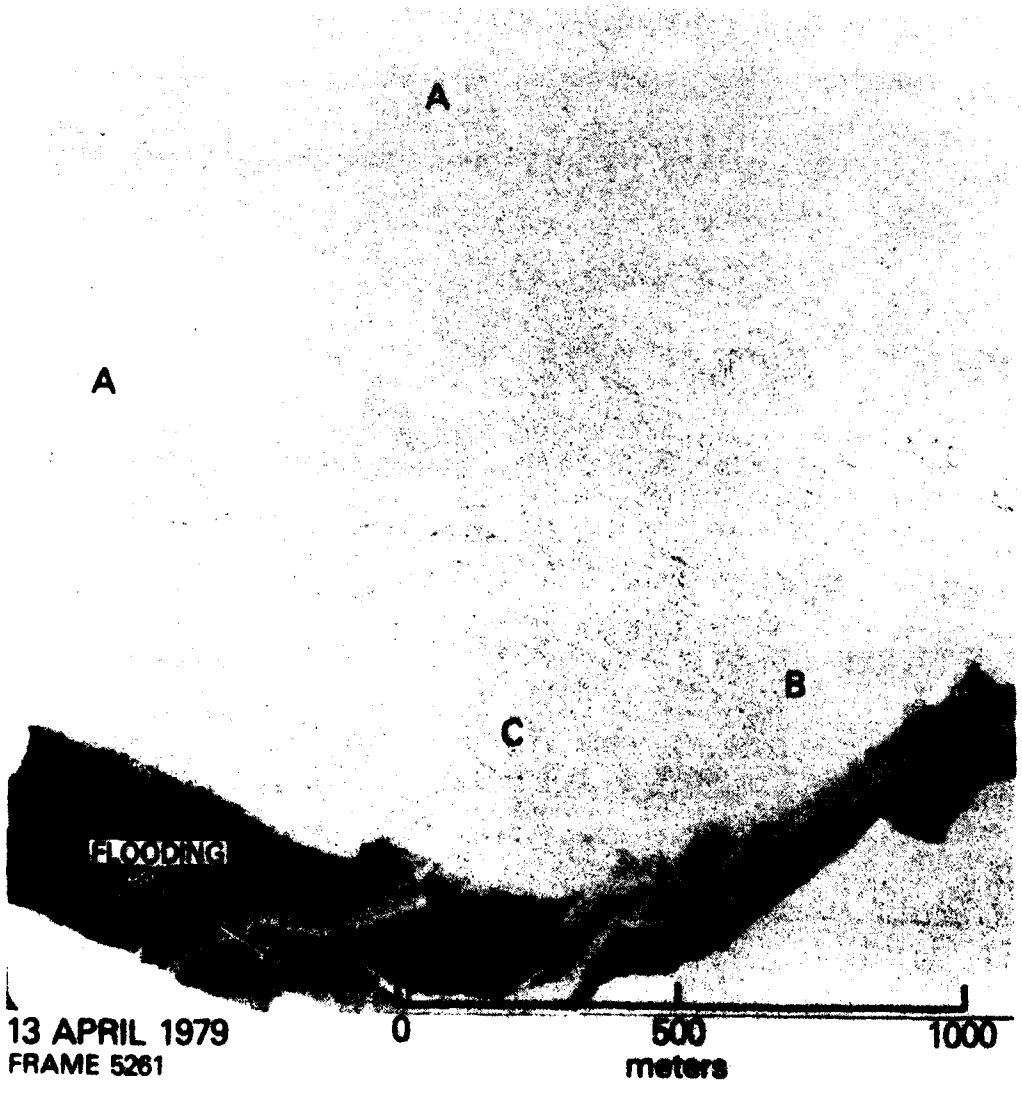

FIGURE 23 AERIAL PHOTOGRAPHY (1524M ALTITUDE) TAKEN IN BAFFIN BAY, 13 APRIL 1979. CORRELATES WITH FIGURE 21 SAR IMAGERY.

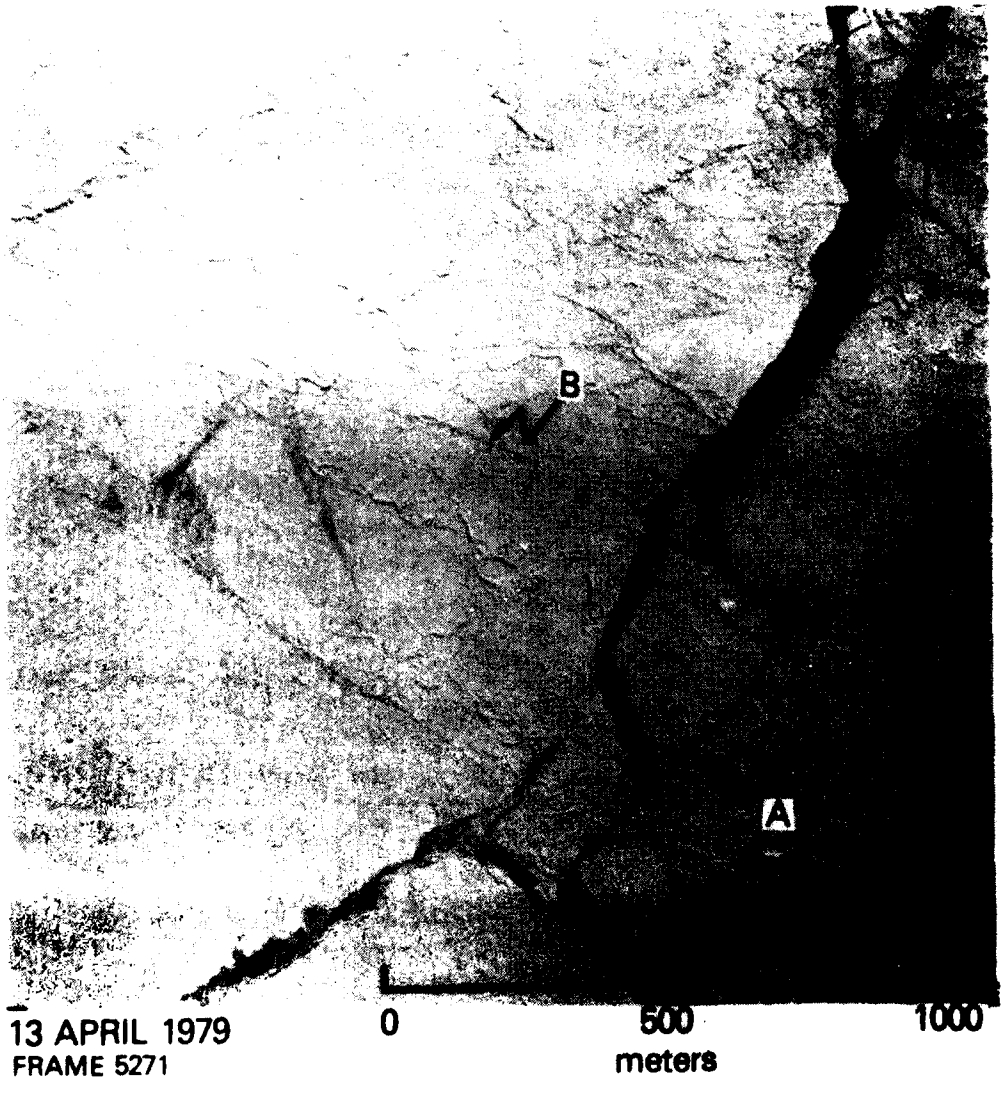

FIGURE 24 AERIAL PHOTOGRAPHY (1524M ALTITUDE) TAKEN IN BAFFIN BAY, 13 APRIL 1979. CORRELATES WITH FIGURE 21 SAR IMAGERY.

UNCLASSIFIED

SECURITY CLASSIFICATION OF THIS PAGE (When Data Entered)

REPORT DOCUMENTATION PAGE	READ INSTRUCTIONS BEFORE COMPLETING FORM
1. REPORT NUMBER: NORDA Technical Note 68 / AD-A090 629	2. GOVT ACCESSION NO. / 3. RECIPIENT'S CATALOG NUMBER
4. TITLE (and Subtitle): Eastern Arctic SURSAT SAR Ice Experiment: Radar Signatures of Sea Ice Features	5. TYPE OF REPORT & PERIOD COVERED
	6. PERFORMING ORG. REPORT NUMBER
7. AUTHOR(s): R. D. Ketchum, Jr. L. Dennis Farmer	8. CONTRACT OR GRANT NUMBER(s)
9. PERFORMING ORGANIZATION NAME AND ADDRESS: Naval Ocean Research and Development Activity Ocean Science and Technology Laboratory NSTL Station, Mississippi 39529	10. PROGRAM ELEMENT, PROJECT, TASK AREA & WORK UNIT NUMBERS
11. CONTROLLING OFFICE NAME AND ADDRESS	12. REPORT DATE: August 1980
	13. NUMBER OF PAGES: 16
14. MONITORING AGENCY NAME & ADDRESS (if different from Controlling Office)	15. SECURITY CLASS. (of this report): UNCLASSIFIED
	15a. DECLASSIFICATION DOWNGRADING SCHEDULE

16. DISTRIBUTION STATEMENT (of this Report)

Unlimited

17. DISTRIBUTION STATEMENT (of the abstract entered in Block 20, if different from Report)

18. SUPPLEMENTARY NOTES

19. KEY WORDS (Continue on reverse side if necessary and identify by block number)

Steep angle synthetic aperature radar (SAR)
Sea ice imagery

20. ABSTRACT (Continue on reverse side if necessary and identify by block number)

Evaluation of X- and L-band steep angle synthetic aperture radar (SAR) sea ice imagery taken in Baffin Bay and Davis Strait in April 1979 has shown that description and discrimination of first-season ice types can be difficult because of ambiguous radar returns. Ambiguous returns seen on X-band radar imagery are attributed to snow cover. The data have indicated that changes in snow properties due to melting and refreezing cause development of a highly reflective medium to the 3 cm X-band radar. The 25 cm L-band radar is not

DD FORM 1 JAN 73 1473 EDITION OF 1 NOV 65 IS OBSOLETE
S/N 0102-LF-014-6601

UNCLASSIFIED

SECURITY CLASSIFICATION OF THIS PAGE (When Data Entered)

noticeably affected by the observed phenomena, thus correlation of coincident X- and L-band imagery often resolves interpretation ambiguities on the X-band imagery caused by the snow effects.

The data suggest that L-band radar energy often penetrates the ice and that subsurface returns are received. These returns also produce ambiguities in interpretation. Apparent smooth surfaces do not show this effect, but rough surfaces which have widely different roughness densities may produce apparently equal backscatter of L-band radar.

Ice ridge identification and discrimination was often poor due to the obscuring effects of background clutter associated with the above-suggested backscattering phenomena. Small ridge sizes versus system resolution and steep angles of incidence also reduce ridge identification capabilities.

Some icebergs produced time-delayed L-band signals, indicating internal reflections within the iceberg. Iceberg/water interface reflections rather than volume scattering are indication. L-band radar cannot be depended upon for iceberg identification, since icebergs may be only partially imaged or not imaged at all by this frequency.